nature

https://doi.org/10.1038/s41586-022-04466-x

Accelerated Article Preview

Memory B cell repertoire from triple vaccinees against diverse SARS-CoV-2 variants

Received: 22 December 2021

Accepted: 20 January 2022

Accelerated Article Preview
Published online: 28 January 2022

Cite this article as: Wang, K. . et al. Memory B cell repertoire from triple vaccinees against diverse SARS-CoV-2 variants. *Nature* https://doi.org/10.1038/s41586-022-04466-x (2022).

Kang Wang, Zijing Jia, Linlin Bao, Lei Wang, Lei Cao, Hang Chi, Yaling Hu, Qianqian Li, Yinan Jiang, Qianhui Zhu, Yongqiang Deng, Pan Liu, Nan Wang, Lin Wang, Min Liu, Yurong Li, Boling Zhu, Kaiyue Fan, Wangjun Fu, Peng Yang, Xinran Pei, Zhen Cui, Lili Qin, Pingju Ge, Jiajing Wu, Shuo Liu, Yiding Chen, Weijin Huang, Cheng-Feng Qin, Youchun Wang, Chuan Qin & Xiangxi Wang

Publisher: NPG; Journal: Nature: Nature; Article Type: Biology article
MS nr: 10.1038/s41586-022-04466-x

Memory B cell repertoire from triple vaccinees against diverse SARS-CoV-2 variants

Kang Wang,[1,8] Zijing Jia,[1,8] Linlin Bao,[2,8] Lei Wang,[1,7,8] Lei Cao,[1,8] Hang Chi,[3,8] Yaling Hu,[4,8] Qianqian Li,[5,8] Yinan Jiang,[6] Qianhui Zhu,[1,7] Yongqiang Deng,[3] Pan Liu,[1] Nan Wang,[1] Lin Wang,[4] Min Liu,[4] Yurong Li,[4] Boling Zhu,[1] Kaiyue Fan,[1,7] Wangjun Fu,[1,7] Peng Yang,[1,7] Xinran Pei,[1] Zhen Cui,[1,7] Lili Qin,[6] Pingju Ge,[6] Jiajing Wu,[5] Shuo Liu,[5] Yiding Chen,[6] Weijin Huang,[5] Cheng-Feng Qin,[3]† Youchun Wang,[5]† Chuan Qin,[2]† & Xiangxi Wang,[1,7]†

[1]CAS Key Laboratory of Infection and Immunity, National Laboratory of Macromolecules, Institute of Biophysics, Chinese Academy of Sciences, Beijing 100101, China.

[2]Key Laboratory of Human Disease Comparative Medicine, Chinese Ministry of Health, Beijing Key Laboratory for Animal Models of Emerging and Remerging Infectious Diseases, Institute of Laboratory Animal Science, Chinese Academy of Medical Sciences and Comparative Medicine Center, Peking Union Medical College, Beijing, China.

[3]State Key Laboratory of Pathogen and Biosecurity, Institute of Microbiology and Epidemiology, Academy of Military Medical Sciences, Beijing, China.

[4]Sinovac Biotech Ltd, Beijing, China.

[5]Division of HIV/AIDS and Sex-Transmitted Virus Vaccines, Institute for Biological Product Control, National Institutes for Food and Drug Control (NIFDC), Beijing 102629, China.

[6]Acrobiosystems Inc, Beijing, China.

[7]University of Chinese Academy of Sciences, Beijing 100049, China.

[8]These authors contributed equally: Kang Wang, Zijing Jia, Linlin Bao, Lei Wang, Lei Cao, Hang Chi, Yaling Hu, Qianqian Li.

†**e-mail:** qincf@bmi.ac.cn; wangyc@nifdc.org.cn; qinchuan@pumc.edu.cn; xiangxi@ibp.ac.cn

Omicron, the most heavily mutated SARS-CoV-2 variant so far, is highly resistant to neutralizing antibodies, raising unprecedented concerns about the effectiveness of antibody therapies and vaccines [1,2]. We examined whether sera from individuals who received two or three doses of inactivated vaccine, could neutralize authentic Omicron. The seroconversion rates of neutralizing antibodies were 3.3% (2/60) and 95% (57/60) for 2- and 3-dose vaccinees, respectively. For three-dose recipients, the geometric mean neutralization antibody titre (GMT) of Omicron was 16.5-fold lower than that of the ancestral virus (254). We isolated 323 human monoclonal antibodies (mAbs) derived from memory B cells in 3-dose vaccinees, half of which recognize the receptor binding

domain (RBD) and show that a subset of them (24/163) neutralize all SARS-CoV-2 variants of concern (VOCs), including Omicron, potently. Therapeutic treatments with representative broadly neutralizing mAbs were highly protective against SARS-CoV-2 Beta and Omicron infections in mice. Atomic structures of the Omicron Spike in complex with three types of all five VOC-reactive antibodies defined the binding and neutralizing determinants and revealed a key antibody escape site, G446S, that confers greater resistance to one major class of antibodies bound at the right shoulder of RBD through altering local conformation at the binding interface. Our results rationalize the use of 3-dose immunization regimens and suggest that the fundamental epitopes revealed by these broadly ultrapotent antibodies are a rational target for a universal sarbecovirus vaccine.

The ongoing evolution and emergence of severe acute respiratory syndrome coronavirus 2 (SARS-CoV-2) variants raise concerns about the effectiveness of monoclonal antibodies (mAbs) therapies and vaccines [3-5], posing challenges for global pandemic control. These variants were characterized as Variant of Interest, VOI or Variant of Concern, VOC by the World Health Organization (WHO). The more recently identified Omicron variant (B.1.1.529), designated as a new VOC, has led to an unprecedented surge in COVID-19 cases in South Africa and is now spreading across the world [6]. Remarkably, Omicron is the most heavily mutated variant to emerge so far with over thirty mutations in spike (S) protein, fifteen of which occur in the receptor binding domain (RBD). In addition, there are three small deletions and one 3-residue insertion in the N-terminal domain (NTD) of S1 subunit (Fig. 1a). The pattern of some of these alterations, similar to the those noted in previous VOCs, such as Δ69-70 in Alpha, N501Y in Alpha, Beta and Gamma, P681H in Alpha and Delta, are presumably associated with enhanced transmissibility, while many substitutions, including G142D/Δ143-145, ins214EPE, K417N, T478K, E484A, Q493R and N501Y, are closely related with resistance to neutralizing antibodies and vaccine induced humoral immunity [3,5,7-11] (Fig. 1a and 1b).

Although COVID-19 vaccines continued to be effective against severe diseases and deaths, including those caused by the circulating Delta variant, waning immunity and massive breakthrough infections caused by viral diversification warrant the need for a third dose or new vaccines. To combat the current resurgence of the

epidemic, the U.S. Food and Drug Administration has authorized use of a 3rd booster dose for all adults after completion of primary vaccination with approved COVID-19 vaccine [12]. This step seems essential because preliminary studies have indicated that three doses of Pfizer-BioNtech mRNA vaccine neutralize the Omicron variant with an approximate 40-fold decline, while two doses are less effective [1,13]. However, these preliminary data on the neutralization sensitivity of Omicron require further independent confirmation. The clinical impact of natural and vaccine-induced immunity with regards to protection from infection and severe disease needs urgent investigation.

Authentic Omicron neutralization

The CoronaVac, a β-propiolactone-inactivated vaccine against COVID-19, has been approved for emergency use, and recommended for a booster dose (third) of inactivated vaccine in older persons by WHO [14,15]. Serum specimens from two groups of 2-dose (n=60, at month 0, 1) or 3-dose (n=60, at months 0, 1, 7) CoronaVac vaccinee volunteers were collected for evaluating neutralization titers against the Omicron and Delta variants using a live SARS-CoV-2. None of the volunteers recruited for vaccination was infected by SARS-CoV-2 prior to the study. Blood samples from vaccinees collected 4 weeks after the last vaccination were used in this study, to compare NAb titers against circulating SARS-CoV-2 variants. An early passage of isolated (CHK06 strain) and sequence confirmed live Omicron virus was used for neutralization assay in this study. Among three doses of CoronaVac recipients, the geometric mean half-maximal neutralizing titers (GMT NT_{50}) against live wild-type (WT) virus, Delta and Omicron variants were 253.9, 77.8 and 15.4, respectively. Compared with WT, neutralizing titers against Delta and Omicron were, on average, 3.3-fold and 16.5-fold reduced, respectively (Fig. 1c). Only 3 of 60 samples had a NT_{50} titer of < 8 against the Omicron with a seroconversion rate of 95% for neutralizing antibodies (Fig. 1c). However, it's more concerning about effectiveness for two-dose regime against Omicron infection. Among two doses of CoronaVac recipients, NT_{50} titer against Delta was 6.6 with a 5.1-fold reduction when compared to WT, but none of the serum specimens had an NT_{50} titer of >8 against Omicron (Fig. 1c). Compared to 2-dose vaccinees, sera of the 3-dose vaccinees displayed lower reduction in neutralization titers against Delta, which is consistent

with previous observations that 3-dose administration of inactivated vaccine leads to enhanced neutralizing breadth to SARS-CoV-2 variants [7].

MAbs elicited by 3-dose vaccination

We previously sorted immunoglobulin (IgG+) memory B cells from peripheral blood mononuclear cells (PBMCs) of four 3-dose CoronaVac vaccinees using prefusion SARS-CoV-2 S as a bait [7,16]. In total, we sorted 1,800 SARS-CoV-2 S-specific memory B cells, obtained 422 paired heavy- and light-chain antibody sequences, and selected 323 antibodies for expression (Supplementary Table 1). Characterization by ELISA showed that 163, 100 and 51 recognized the RBD, NTD and S2, respectively and 9 failed to bind S (Fig. 2a). Biolayer interferometry affinities (BLI) measurements showed that nearly all RBD-directed antibodies bound to WT SARS-CoV-2 at sub-nM levels (Supplementary Table 1) and 127 of them showed neutralization activities against both authentic and pseudotyped WT SARS-CoV-2 were selected for further investigation. Of these antibodies, over 93% of these antibodies exhibited broad binding activities to most VOCs and VOIs (Supplementary Table 1). Notably, 85% of these antibodies cross-reacted with the Omicron RBD (Supplementary Table 1). Contrarily, ~80% of NTD antibodies lost their associations with Omicron. Additionally, NTD antibodies also showed relatively poor cross-reactivity to other four VOCs due to the greater diversity of the NTD (Fig. 1a, b and Supplementary Table 1).

MAbs with broad neutralization

Results of the pseudovirus neutralization assays performed by carrying the S of WT or other VOCs [17,18] identified 31 RBD targeting antibodies that were especially potent with their half-maximal inhibitory concentration (IC_{50}) ranging from 0.002 to 0.800 μg/ml against WT as well as all VOCs (Fig. 2b). Among these, 30 antibodies executed their neutralization via directly blocking the interactions between the RBD and its receptor hACE2, while 1 antibody employs other mechanisms to neutralize viral infection (Fig. 2c, Extended Data Fig. 1). Especially, a subset of RBD antibodies (13 and 24) neutralized Omicron with $IC_{50} < 0.02$ and 0.1 μg/ml, respectively. These neutralizations are as potent as those exhibited by best-in-class antibodies against WT (Fig. 2b and 2d, Supplementary Table 1, 2). We obtained IC_{50} values of 0.27 and 0.16 μg/ml for well-studied therapeutic antibodies like VIR-7831 and DXP-604,

respectively. These values are 10~40-fold higher than those of the subset antibodies (Extended Data Fig. 2, Supplementary Table 1). Concerningly, some antibody drugs, such as REGN10933, REGN10987, LY-CoV555, LY-CoV016, AZD1061 and AZD8895, almost lost their neutralization activities against Omicron (Extended Data Fig. 2, Supplementary Table 1)[2]. Meanwhile, specific VOC-resistant antibodies with high neutralizing potency against WT and some other VOCs (IC_{50} <0.2 μg/ml) were identified and these comprise ~30% of the antibody repertoire (Supplementary Data Table 1). Our previous study revealed that the numbers of nucleotide mutations in the V gene for RBD specific antibodies in 3-dose vaccinees were substantially higher than those in 2-dose vaccinees and antibodies obtained from 3-dose vaccinees possessed higher binding activities than those from 2-dose vaccinated individuals[5], which indicates the evolution of a wide range of antibodies over time. Experiments repeated using authentic virus, including WT and five circulating VOCs, showed similar neutralization patterns by all these antibodies (Extended Data Fig. 3), further verifying the neutralizing potency and breadth for this subset of antibody repertoire elicited by 3-dose vaccination.

Structures of Omicron S trimer and mAbs

Antibodies targeting the RBD can be categorized into six general classes (from I to VI) based on cluster analysis on epitope from 265 available RBD-NAb complex structures [7], that are related to the four groups on the basis of competition with the hACE2 for binding to S and recognition of the up or down state of the three RBDs in S [19-21]. ELISA-based square competition matrix analysis with the aid of existing structural data revealed the presence of 3 major groups in this subset of antibody repertoire (Extended Data Fig. 4). To delineate the structural basis for antibody-mediated neutralization, we determined the cryo-EM structure of a prefusion stabilized Omicron S trimer in complex with representative Fab fragments. The two highly potent antibodies against Omicron (XGv347 and XGv289 with IC_{50} values of 0.006 and 0.016 μg/ml, respectively), one mAb (XGv282 with IC_{50} of 0.268 μg/ml) with median neutralizing activities against Omicron, but high neutralizing potency against other four VOCs, and one mAb (XGv265 with IC_{50} of 7.479 μg/ml) with >500-fold decreased neutralization against Omicron, but potent neutralization against other four VOCs were selected for structural investigations (Fig. 2b). We determined cryo-EM reconstructions of these complexes at 3.3 – 3.8 Å, and performed local

refinement to further improve the densities around the binding interface between RBD and antibodies, enabling reliable analysis of the interaction details (Fig. 3, Extended Data Fig. 5, 6 and 7, Extended Data Table 1).

The XGv347-Omicron S complex structures revealed three distinct conformational states: three XGv347 Fabs bound to a completely closed S with three down RBDs; two XGv347 Fabs bound to either two or one up and one down RBDs on S (Fig. 3a). By contrast, each of the complex structures for XGv289, XGv282 and XGv265 showed only one configuration where three XGv289 Fabs bound to two up and one down RBDs; three XGv282 Fabs bound to one up and two down RBDs; two XGv265 Fabs bound to S trimer with one down and one up RBD, although the XGv265-bound up RBD conformation was weakly resolved and therefore not modeled (Fig. 3a). Antibody XGv347 binds to an epitope at the tip of RBD, largely overlapping with the patch targeted by ACE2 (Fig. 2c, 3b, 3c, Extended Data Fig. 1). Structural comparisons revealed that XGv347 is very similar to A23-58.1, an ultrapotent and broadly reactive NAb effective against 23 SARS-CoV-2 variants [22], but significant differences could be observed in the CDR domains (Extended Data Fig. 8). Furthermore, the residues of the epitope of XGv347 match with a major subset of those targeted by S2K146, another broadly cross-reactive sarbecovirus NAb [23,24], highlighting a plausible capability of these NAbs to cross-neutralize Omicron and circulating SARS-CoV-2 variants. Unexpectedly, the epitopes of XGv347, A23-58.1 as well as their sister NAbs would be normally inaccessible for the RBD-down conformation in the WT S, but become accessible for either up or down RBDs in the Omicron S due to a markedly outward expansion and a ~10º clockwise rotation of three RBDs, leading to an approximately 9 Å conformational movement for RBM (Fig. 3d and Extended Data Fig. 9). The XGv347 paratope constituted five complementarity determining regions (CDRs) with heavy chain and light chain contributing 70% and 30% of the binding surface area, respectively (Fig. 3b, 3c and Extended Data Table 2). Overall XGv289, XGv282 and XGv265 bind patches surrounding the right shoulder of RBD with various orientations [20], but in a manner similar to those observed for DH1047, BD-812 and REGN10987; antibodies known to generally neutralize most VOCs with high potency [25-27], but showing declined, to varying degrees, binding and neutralizing activities against Omicron due to the presence of new N440K and G446S mutations (Fig. 2b, Extended Data Fig. 10 and

Extended Data Table 2). Notably, XGv265 and REGN10987 recognize almost same epitopes, both nearly losing their neutralizing activities against Omicron, despite retaining weak binding (Extended Data Fig. 10). Structural superimpositions and competitive BLI assays reveal that XGv347 and either XGv289 or XGv265 can simultaneously bind to S, informing strategies to rationally design two-antibody combinations for potential therapeutics (Extended Data Fig. 11, Extended Data Fig. 12).

Structural basis for immune escape

XGv347, XGv289, XGv282 and XGv265 bound Omicron with 5-40 folds lower affinity compared to their binding with WT, although the same binding modes for two orthologs were observed (Fig. 3 and Supplementary Table 1). For XGv347, tight binding to WT S is primarily due to extensive hydrophobic interactions contributed by F456, Y473, F486 and Y489 from WT RBD, V32, V53, W51, P100 and F111 from heavy chain, and Y33 from light chain, and 9 hydrogen bonds (Extended Data Fig. 13 and Table 3). Hydrophobic interactions between the Omicron RBD and XGv347 are largely maintained. However, substitutions of Y505H and K417N abolish three hydrogen bonds forged with K75, D31 and E104 from HCDRs, leading to conformational shifts in HCDR3 and the RBM tip (residues 470-490), which further perturb six hydrogen bonds built by Y473, A475, S477, T478, Q493 from WT RBD with T105, C107, A56, G55 and D109 from HCDRs, albeit with an extra hydrogen bond established by the mutation Q493R and G55 from HCDR2 in Omicron (Extended Data Fig. 13). Similarly, a large patch of hydrophobic interactions constructed by V445, G446, Y449, P499 from WT RBD and F33, L50, I51, Y59, W103 from HCDRs as well as extensive hydrophilic interactions facilitate tight binding between XGv289 and WT S (Fig. 3 and Extended Data Fig. 13). Substitution of G446S disrupts the hydrophobic microenvironment, substantially decreasing hydrophobic interactions between Omicron S and XGv289. Furthermore, mutations of N440K and Q498R, together with altered local conformation, also lessen hydrogen bonds formed by N439, K440, Y449, R498, T500, Q506 from Omicron RBD and D95, L98 from LCDRs as well as Y59, N62 from HCDRs that would exist in XGv289-WT S complex (Extended Data Fig. 13). Among these four representative antibodies, XGv282 showed minimal reduction in binding affinity (5-fold), but remarkable reduction in neutralization (~40-fold), versus the characterization of

XGv347 with 40-fold decrease in binding, but unchanged neutralization against Omicron when compared to WT (Extended Data Table 3), suggesting that epitope, rather than binding affinity, might play more crucial roles in the neutralizing potency and breadth of an antibody. Consistent with XGv289, the substitution of G446S alters the hydrophobic microenvironment generally established by RBD and a group of antibodies bound at the right shoulder, including XGv289 and XGv282, triggering a conformational shift on CDRs and disrupting antibody recognition (Extended Data Fig. 13). In addition, the mutation E484A breaks hydrogen bond-connection with R74 from XGv282 HCDR2 and losses of charge interactions between R346, K444 from WT RBD and D56, D58 of XGv265 LCDR2 due to conformational alterations, further decreasing the binding of XGv282 and XGv265 to the Omicron variant, respectively (Extended Data Fig. 13). Taken together, G446S, acting as a critical mutation site, can alter the local conformation at the binding interface, conferring greater resistance to one class of antibodies bound at the right shoulder of RBD.

The therapeutic activities of mAbs

Given the excellent neutralizing breadth and potency at cell-based levels for above antibodies, we next sought to assess the correlation between *in vitro* neutralization and *in vivo* protection. A number of representative mAbs with high neutralizing potency and breadth, belonging to different classes, such as XGv347, XGv289, XGv282, XGv265 and XGv052, produced in the HEK293F cell line were selected for therapeutic evaluation in a well-established mouse model challenged with the Beta variant [28]. Upon Beta intranasal challenge, adult BALB/c showed robust viral replication in the lungs at 3-5 days post inoculation (dpi). To evaluate the protection efficacy of these mAb, BALB/c mice challenged with the Beta variant were administered a single dose of as low as 5 mg/kg of XGv347, XGv289, XGv282, XGv265 and XGv052 individually or combinations of XGv282 and XGv347 (2.5 mg/kg for each), and XGv052 and XGv289 (2.5 mg/kg for each) in therapeutic settings (Fig. 4a). Heavy viral loads with high levels of viral RNAs (> 10^9 copies/g) were detected in the lungs at day 5 post-infection in the control group of mice treated with PBS. However, a single dose of XGv282 reduced the viral RNA loads by ~10,000-fold in the lungs compared to the control group (Fig. 4b). Remarkably, a single dose of XGv289, XGv265, XGv347, XGv052 or antibody cocktails of XGv282 and XGv347, XGv052 and XGv289 resulted in a complete clearance of viral particles

in the lungs (Fig. 4b, 4c). A potential synergistic effect was observed for combined therapies of XGv282 + XGv347 at 2.5 mg/kg for each (Fig. 4b, 4c). In addition, histopathological examination revealed severe interstitial pneumonia, characterized by alveolar septal thickening, inflammatory cell infiltration and distinctive vascular system injury developed in mice belonging to the control group at day 5 (Fig. 4d). In contrast, no obvious lesions of alveolar epithelial cells or focal hemorrhage were observed in the lung sections from mice that received indicated antibody treatments (Fig. 4d, Extended Data Fig. 14). To further evaluate whether XGv347 could serve as therapeutic interventions against Omicron *in vivo*, we tested the protective efficacy of XGv347 on hACE2 transgenic mice challenged by Omicron. We recorded the body weight for each mouse daily after infection for 5 days and found that the therapeutic treatment group maintained their body weight, whereas the control group substantially lost weight (Fig. 4e), indicating that XGv347 applied after the infection could greatly improve the physiological condition of the Omicron-infected mice. Similar to the studies with the Beta strain of mice, therapeutic administration of XGv347 conferred a clear benefit on the hACE2 transgenic mouse model (K18-hACE2) [29] as indicated by a complete clearance in viral RNA loads in the lungs and trachea at day 5 post Omicron challenge (Fig. 4f). More importantly, K18-hACE2 mice infected with Omicron developed moderate interstitial pneumonia characterized by focal to multifocal widen alveolar interstitium accompanied by infiltration of inflammatory cells (Fig. 4g). While, no obvious pathological injury was observed in the lung from mice that received XGv347 treatments (Fig. 4g). Collectively, these results suggest that some of the antibodies, at least best-in-class antibodies like XGv347, from the repertoire elicited by a 3-dose vaccination regimen retain therapeutic potential against currently circulating VOCs.

Discussion

The ongoing pandemic has witnessed frequent occurrences of SARS-CoV-2 variants that increase transmissibility and reduce potency of vaccine-induced and therapeutic antibodies [4,30]. More recently, there has been unprecedented concern that the Omicron variant has significantly increased antibody escape breadth due to newly occurred and accumulated mutations in the key epitopes of most neutralizing antibodies. Alarmingly, Omicron nearly ablates the neutralization activity of most FDA approved antibody drugs, including LY-CoV555, LY-CoV016, REGN10933, REGN10987,

AZD8895 and AZD1061 [2]. These issues raise an urgent need to develop next-generation antibody-based therapeutics that can broadly neutralize these variants, as well as future variants of concern. Our previous study revealed that the regimen of 3-dose vaccination (0, 1, 7 months) of inactivated vaccine leads to an improved immunity response with significantly enhanced neutralizing breadth via ongoing antibody somatic mutation and memory B cell clonal turnover [7,31]. Correlated with this, one subset of highly potent neutralizing antibodies with broad activities (IC_{50} < 0.2 μg/ml) against all circulating VOCs, including Omicron, were present in at least four individuals who had received three doses of inactivated ancestral SARS-CoV-2 vaccine. Some, but not limited to these of this subset antibodies protected against Beta and Omicron infections in mice. Furthermore, our structural and functional analyses revealed that a newly occurred mutation, G446S, might act as a critical antibody escape site, conferring greater resistance to one major class of antibodies bound at the right shoulder of RBD via altering microenverionments at the S-NAb binding interface.

In addition to evading currently available antibody therapeutics, the Omicron variant can diminish the efficacy of all clinically approved vaccines, including the mRNA vaccines and inactivated vaccines [30,32]. There is an ongoing debate about whether the immune responses can be fine-turned to the Omicron variant by boosting with a tweaked (Omicron-based) vaccine. A major hurdle for this approach is the "original antigenic sin", a phenomenon documented in some other infectious diseases, including flu [33]. The presence of a subset of antibodies with broad neutralizing activities against all circulating VOCs in memory B-derived antibody repertoire from the 3-dose vaccinees suggests a possibility that selective and expeditious recall of humoral responses might be elicited via the Omicron/future variants infection, conferring to a secondary protection directed by memory etched in the immune system. Further studies are warranted to examine the advantages and disadvantages of booster shots of an Omicron-specific vaccine or simply administration of a booster with the original vaccines. Lastly the identification and characterization of broadly protective antibodies against all circulating VOCs will aid in the development of universal vaccination strategies against sarbecoviruses.

Online content Any methods, additional references, Nature Research reporting summaries, source data, extended data, supplementary information, acknowledgements, peer review information; details

of author contributions and competing interests; and statements of data and code availability are available at [Article DOI].

Received 22 December 2021; accepted 20 January 2022

1 Carreno, J. M. et al. Activity of convalescent and vaccine serum against a B. 1.1. 529 variant SARS-CoV-2 isolate. nature, doi:https://doi.org/10.1038/d41586-021-03846-z (2021).

2 Cao, Y. R. et al. B. 1.1. 529 escapes the majority of SARS-CoV-2 neutralizing antibodies of diverse epitopes. nature (2021).

3 Mlcochova, P. et al. SARS-CoV-2 B. 1.617. 2 Delta variant replication and immune evasion. Nature, 1-6 (2021).

4 Wang, G.-L. et al. Susceptibility of circulating SARS-CoV-2 variants to neutralization. New England Journal of Medicine (2021).

5 Altmann, D. M., Boyton, R. J. & Beale, R. Immunity to SARS-CoV-2 variants of concern. Science 371, 1103-1104 (2021).

6 Karim, S. S. A. & Karim, Q. A. Omicron SARS-CoV-2 variant: a new chapter in the COVID-19 pandemic. The Lancet (2021).

7 Wang, K. et al. A third dose of inactivated vaccine augments the potency, breadth, and duration of anamnestic responses against SARS-CoV-2. medRxiv (2021).

8 Hastie, K. M. et al. Defining variant-resistant epitopes targeted by SARS-CoV-2 antibodies: A global consortium study. Science 374, 472-478 (2021).

9 Yuan, M. et al. Structural and functional ramifications of antigenic drift in recent SARS-CoV-2 variants. Science (2021).

10 Zhang, J. et al. Membrane fusion and immune evasion by the spike protein of SARS-CoV-2 Delta variant. Science, eabl9463 (2021).

11 Saito, A. et al. Enhanced fusogenicity and pathogenicity of SARS-CoV-2 Delta P681R mutation. Nature, 1-10 (2021).

12 Mbaeyi, S. et al. The Advisory Committee on Immunization Practices' Interim Recommendations for Additional Primary and Booster Doses of COVID-19 Vaccines—United States, 2021. Morbidity and Mortality Weekly Report 70, 1545 (2021).

13 Garcia-Beltran, W. F. et al. mRNA-based COVID-19 vaccine boosters induce neutralizing immunity against SARS-CoV-2 Omicron variant. Cell, doi:https://doi.org/10.1038/d41586-021-03846-z (2021).

14 Gao, Q. et al. Development of an inactivated vaccine candidate for SARS-CoV-2. Science 369, 77-81 (2020).

15 Hasan, S. A. W. Interim statement on booster doses for COVID-19 vaccination. Update 4 (2021).

16 Wang, Z. et al. mRNA vaccine-elicited antibodies to SARS-CoV-2 and circulating variants. Nature 592, 616-622 (2021).

17 Lv, Z. et al. Structural basis for neutralization of SARS-CoV-2 and SARS-CoV by a potent therapeutic antibody. Science 369, 1505-1509 (2020).

18 Yao, H. et al. Rational development of a human antibody cocktail that deploys multiple functions to confer Pan-SARS-CoVs protection. Cell research 31, 25-36 (2021).

19 Barnes, C. O. et al. SARS-CoV-2 neutralizing antibody structures inform therapeutic strategies. Nature 588, 682-687 (2020).

20 Dejnirattisai, W. et al. The antigenic anatomy of SARS-CoV-2 receptor binding domain. Cell 184, 2183-2200. e2122 (2021).

21 Tong, P. et al. Memory B cell repertoire for recognition of evolving SARS-CoV-2 spike. Cell 184, 4969-4980 e4915, doi:10.1016/j.cell.2021.07.025 (2021).

22 Wang, L. et al. Ultrapotent antibodies against diverse and highly transmissible SARS-CoV-2 variants. Science 373, eabh1766 (2021).

23 Park, Y.-J. et al. Antibody-mediated broad sarbecovirus neutralization through ACE2 molecular mimicry. Biorxiv (2021).

24 Cameroni, E. et al. Broadly neutralizing antibodies overcome SARS-CoV-2 Omicron antigenic shift. bioRxiv (2021).

25 Martinez, D. R. et al. A broadly cross-reactive antibody neutralizes and protects against sarbecovirus challenge in mice. Science translational medicine, eabj7125 (2021).

26 Zhu, L. et al. Double lock of a potent human therapeutic monoclonal antibody against SARS-CoV-2. National Science Review 8, nwaa297 (2021).

27 Hansen, J. et al. Studies in humanized mice and convalescent humans yield a SARS-CoV-2 antibody cocktail. Science 369, 1010-1014 (2020).

28 Chen, Q. et al. Transient acquisition of cross-species infectivity during the evolution of SARS-CoV-2. National science review 8, nwab167 (2021).

29 Bao, L. et al. The pathogenicity of SARS-CoV-2 in hACE2 transgenic mice. Nature 583, 830-833 (2020).

30 Wilhelm, A. et al. Reduced Neutralization of SARS-CoV-2 Omicron Variant by Vaccine Sera and monoclonal antibodies. medRxiv (2021).

31 Wang, Z. et al. Naturally enhanced neutralizing breadth against SARS-CoV-2 one year after infection. Nature 595, 426-431 (2021).

32 Gardner, B. J. & Kilpatrick, A. M. Estimates of reduced vaccine effectiveness against hospitalization, infection, transmission and symptomatic disease of a new SARS-CoV-2 variant, Omicron (B. 1.1. 529), using neutralizing antibody titers. medRxiv (2021).

33 Biswas, A., Chakrabarti, A. K. & Dutta, S. Current challenges: from the path of “original antigenic sin” towards the development of universal flu vaccines: Flu vaccine efficacy encounters significant hurdles from pre-existing immunity of the host suggesting assessment of host immunity before vaccination. International reviews of immunology 39, 21-36 (2020).

34 Cui, Z. et al. Structural and functional characterizations of altered infectivity and immune evasion of SARS-CoV-2 Omicron variant. bioRxiv (2021).

Methods

Facility and ethics statements

All procedures associated with SARS-CoV-2 live virus were approved by the Animal experiment Committee Laboratory Animal Center, Beijing Institute of Microbiology

and Epidemiology with an approval number of IACUC-IME-2021-022 and performed in Biosafety Level 3 (BSL-3) laboratories in strict accordance with the recommendations in the Guide for Care and Use of Laboratory Animals. The procedures about human participants were approved by the Ethics Committee (seal) of Beijing Youan Hospital, Capital Medical University with an approval number of LL-2021-042-K. All participants were provided written informed consent.

Viral stock and cell lines

SARS-CoV-2 WT strain CN01 was originally isolated from a patient during the early phase of COVID-19 endemic in China. SARS-CoV-2 variant of concern (VOC) Beta (B.1.351 lineage) strain GDPCC was isolated in a patient from South Africa and an Omicron (B.1.1.529 lineage) strain was isolated from a patient in Hong Kong and now preserved in SinoVac Biotech Ltd. All virus strains were first purified by standard plaque assay as previously described[14] and then inoculated into Vero cells (CCL-81) grown to 95% in 10% fetal bovine serum (FBS) supplemented Dulbecco's minimal essential medium (DMEM) for amplification.

Human sera samples

The serum samples were obtained from healthy volunteers who had no history of COVID-19 and were verified by PCR and serological assay and received two doses or three doses of CoronaVac (Sinovac) inactivated vaccine specific against SARS-COV-2. The whole study was conducted in accordance with the requirements of Good Clinical Practice of China.

Authentic virus neutralization assay

The serum samples were first incubated at 56 ℃ for 30 min for inactivation. The heat-treated samples or monoclonal antibodies (mAbs) were subject to seral dilution from 1: 4 or 50 μg/ml with DMEM in two-fold steps and mixed with a virus suspension containing 100 $TCID_{50}$ at 36.5℃ for 2h, after which, the mixtures were added to wells seeded with confluence Vero cells and incubated at 36.5℃ for another 5 days in a humidified 5% CO_2 cell incubator. After that, the cytopathic effect (CPE) of each well was observed under microscopes by three different individuals and the related dilutions and concentrations were recorded and used for the titration of samples tested by the method of Reed-Muench[14].

Pseudovirus neutralization assay

The pseudotyped viruses bearing the S protein were generated, aliquoted and restored as previously described[18]. Briefly, 293T cells were first transfected with the plasmid embedded with the S gene of WT or VOC/VOI (Alpha, Beta, Gamma, Delta, Lamda and Omicron) SARS-CoV-2. The transfected 293T cells were infected with VSV G pseudotyped virus (G*ΔG-VSV) at a multiplicity of infection (MOI) of 4. After incubation for five hours, cells were washed with PBS, and then complete culture medium was added. After another 24 hours, the SARS-CoV-2 pseudoviruses were produced and harvested. For the *In vitro* pseudotyped virus neutralization assay, the plasma samples or antibodies were diluted in DMEM starting from 1:10 or 10 μg/ml with 6 additional threefold serial dilutions, each of which were mixed with the harvested pseudovirus and incubated at 37 °C for 1h. After that, the mixtures were added to Huh-7 cells and placed back for incubation for another 24 hours. Then, the luciferase luminescence (RLU) of each well was measured with a luminescence microplate reader. The neutralization percentage was calculated as following: Inhibition (%) = [1- (sample RLU- Blank RLU) / (Positive Control RLU-Blank RLU)] (%). Antibody neutralization titers were presented as 50% maximal inhibitory concentration (IC_{50}).

Protein expression and purification

The sequences of VOC Omicron full-length S protein (residues 1-1208), receptor-binding domain (RBD) (residues 319-541) and N-terminal domain (NTD) (residues 1-304) were modified from the plasmids encoding the S, RBD and NTD of WT SARS-COV-2 (GenBank: MN908947) in our lab by overlapping PCR. In additional to the reported mutations (A67V, Δ69-70, T95I, G142D, Δ143-145, Δ211, L212I, ins214EPE, G339D, S371L, S373P, S375F, K417N, N440K, G446S, S477N, T478K, E484A, Q493R, G496S, Q498R, N501Y, Y505H, T547K, D614G, H655Y, N679K, P681H, N764K, D796Y, N856K, Q954H, N969K, L981F) on Omicron, the proline substitutions at 817, 892, 899, 942, 986 and 987, 'GSAS' substitutions at the S1/S2 furin cleavage site (residues 682-685) and a C-terminal T4 foldon trimerization domain were also introduced in the Omicron S construct to stabilize the trimeric conformation of S protein. For protein expression, the plasmids of these proteins were transiently transfected into HEK293F cells grown in suspension at 37 ℃ in an incubator supplied with 8% CO_2, rotating at 130 rpm. The cell supernatants were

harvested and concentrated three days post-transfection, and further purified by affinity chromatography using resin attached with streptavidin and size-exclusion chromatography (SEC) using a Superose 6 10/300 column (GE Healthcare Life Sciences) equilibrated with the buffer containing 20 mM Tris-HCl, pH 8.0, and 200 mM NaCl.

Single memory B cell isolation and sequencing

PBMCs were separated from the whole-blood samples obtained from four volunteers using Histopaque (Sigma) gradient centrifugation. After washing with Hank's balanced salt solution (HBSS) (Solarbio) for three times, the cells were aliquoted and stored in liquid nitrogen in the presence of FBS and DMSO. For single memory B cell sorting, stored PBMCs were thawed and incubated with CD19 MicroBeads (Miltenyi Biotec) to screen out CD19+ B lymphocytes, which were then incubated with human Fc block (BD Biosciences), anti-CD20-PECy7 (BD1113 Biosciences), S-ECD-PE, and S-ECD-APC. The single memory B cells (CD20-1114 PECy7+ S-ECD-PE+ S-ECD-APC+) were further sorted into 96-well plates using a FACSAria II (BD Biosciences), and followed by sequencing and cloning as previously described[35].

Antibody expression and Fab generation

The selected 323 antibodies were subjected to gene codon optimization and construction with a plasmid encoding human IgG1 Fc as described previously [7]. Then the clones were transiently transfected into mammalian HEK293F cells and incubated for 5 days in a 5% CO_2 rotating incubator at 37°C for antibody expression, which were further purified using protein A and dialyzed into Phosphate Buffered Saline (PBS). The purified mAbs XGv265, XGv282, XGv289 and XGv347 were then processed to obtain their Fab fragments using the Pierce FAB preparation kit (Thermo Scientific) as described previously [36]. Briefly, the samples were first applied to desalination columns to remove the salt and the flow-throughs were collected and incubated with papain that was attached with beads to cleave Fab fragments from the whole antibodies for 5 hours at 37°C. After that, the mixtures were transferred into Protein A columns and the flow-throughs, i.e., the Fab fragments were collected and dialyzed into PBS (ThermoFisher, catalog #10010023).

Bio-layer interferometry

Bio-layer interferometry **(**BLI) experiments were run on an Octet Red 384 machine (Fortebio). To measure the binding affinities of mAbs, monoclonal antibodies were immobilized onto Protein A biosensors (Fortebio) and the threefold serial dilutions of WT RBD, Alpha RBD (ACROBiosystems, Cat No. SPD-C52Hn), Beta RBD (ACROBiosystems, Cat No. SPD-C52Hp), Gamma RBD (ACROBiosystems, Cat No. SPD-C52Hr), Delta RBD (ACROBiosystems, Cat No. SPD-C52Hh) and Omicron RBD (ACROBiosystems, Cat No. SPD-C522e) in PBS were used as analytes. Data were then analyzed using software Octet BLI Analysis 12.2 (Fortebio) with a 1:1 fitting model. For the competitive assay by BLI, SARS-CoV-2 WT RBD tagged with His (ACROBiosystems, Cat No. SPD-C52H3) was loaded on NTA biosensors, which were pre-equilibrated in the buffer for at least 1 min. The loaded biosensors were immersed with the first mAb for 300 s, followed by addition of the second mAb for another 300 s. Data obtained were also analyzed by Octet BLI Analsis 12.2.

ELISA assays

To evaluate whether the given mAbs could block the interaction between human ACE2 (hACE2) and RBD, ACE2 competition ELISA was performed by using the SARS-CoV-2 (B.1.1.529) Inhibitor Screening Kit (ACROBiosystems, Cat No. EP-115) according to the recommended protocol. Briefly, each of the 10 two-fold dilution series of mAbs (starting dilution of 25 μg/ml) and 0.8 μg/ml of HRP-conjugated SARS-CoV-2 RBD were added into the ELISA plate wells which are pre-coated with hACE2 protein. After incubation at 37 ˚C for 1 hour, the plates were washed three times with PBST (0.1% Tween) and the colorimetric signals were developed by addition of 3, 3', 5, 5'-tetramethylbenzidine TMB (Thermo Fisher) for 10 min. The reaction was stopped by addition of 50 μL of 1M H2SO4. The absorbance was measured at 450 nm with an ELISA microplate reader. For each mAb, a blank control with no mAb was added for inhibition calculation. The area under the curve (AUC) of each mAb were determined using Prism V8.0 (GraphPad). For competitive ELISAs to identify the domain of a given mAb, 96-well plates were first coated with RBD (2 μg/ml) and then blocked with 2% BSA in PBS. After incubation with the reference mAbs, the blocking antibody (15 μg/ml), the wells were followed by directly adding the second biotinylated antibodies (0.25 μg/ml). Streptavidin-HRP (BD Biosciences)

was then added for detection. Samples with no first antibody were used as a negative control for normalization.

Cryo-EM sample preparation, data collection

The purified S protein was mixed with each of the Fab fragments of XGv265, XGv282, XGv289 or XGv347 with a molar ratio of 1: 1.2 for 10 s ice incubation, and then dropped onto the pre-glow-discharged holey carbon-coated gold grid (C-flat, 300-mesh, 1.2/1.3, Protochips In.), blotted for 7 seconds with no force in 100% relative humidity and immediately plunged into the liquid ethane using Vitrobot (FEI). Cryo-EM data sets of these complexes were collected at 300 kV with an FEI Titan Krios microscope (FEI). Movies (32 frames, each 0.2 s, total dose of 60 e^{-} $Å^{-2}$) were recorded using a K3 Summit direct detector with a defocus range between 1.5-2.7 μm. Automated single particle data acquisition was carried out by SerialEM, with a calibrated magnification of 22,500 yielding a final pixel size of 1.07 Å.

Cryo-EM data processing

A total of 3,752, 2,631, 3,955 and 5,014 micrographs of S-XGv265-complex, S-XGv282-complex, S-XGv289-complex and S-XGv347-complex, respectively were recorded and subjected to beam-induced motion correction using motionCorr in Relion 3.0 package [37]. The defocus value of each image was calculated by Gctf. Then, 1,302,103, 756,508, 2,332,045 and 2,320,416 particles of the S-XGv265-complex, S-XGv282-complex, S-XGv289-complex and S-XGv347-complex, respectively were picked and extracted for reference-free 2D alignment by cryoSPARC [38], based of which, 422,083, 190,154, 837,832 and 614,852 particles were selected and applied for 3D classification by Relion3.0 for S-XGv265-complex, S-XGv282-complex, S-XGv289-complex and S-XGv347-complex, respectively with no symmetry imposed to produce the potential conformations for the complexes. Afterwards, the candidate model for each complex was selected and processed by non-uniform auto-refinement and postprocessing in cryoSPARC to generate the final cryo-EM density for S-XGv265-complex, S-XGv282-complex, S-XGv289-complex and S-XGv347-complex. To improve the resolution of the interface between RBD and mAbs, the block-based reconstruction was performed to obtain the final resolution of the focused interfaces which contained the interfaces of RBD and mAbs investigated here as described previously [39]. The resolution of each structure was determined on the basis of the gold-standard Fourier shell correlation (threshold = 0.143) and evaluated by

ResMap. All dataset processing is shown in Extended Data Fig. 3 and also summarized in Extended Data Table 2.

Model fitting and refinement

The atomic models of the complexes were generated by first fitting the chains of the native apo SARS-CoV-2 S trimer (PDB number of 6VYB) and Fabs (PDB number of 7LSS and 7CZW for XGv265, 5MES and 5VAG for XGv282, 6UDA and 7MEG for XGv289 as well as 7E3K for XGv347) into the cyo-EM densities of the final S-Fab-complexes described above by Chimera, followed by manually adjustment and correction according to the protein sequences and densities in Coot, as well as real space refinement using Phenix. Details of the refinement statistics of the complexes are summarized in Extended Data Table 2.

MD simulation and ΔG estimation

Model of SARS-CoV-2 WT RBD in complex with XGv265, XGv282, XGv289 and XGv347 were generated in Chimera by superimposition of WT RBD and cryoEM structure of Omicron RBD in complex with the four antibodies. Before molecular dynamics, all models were checked by WHAT IF Web Interface (https://swift.cmbi.umcn.nl/servers/html/index.html) to model missing sidechains and remove atomic clashes. After that, the structure was simulated by GROMACS-2021. Briefly, we used OPLS force field with TIP3P water model to prepare the dynamic system and add Na^+ and Cl^- ions to make the system electrically neutralized. Then, the system was subjected to energy minimization using the steepest descent algorithm until the maximum force of 1,000 kJ mol-1 has been achieved. NVT ensemb1e via the Nose-Hoover method at 300 K and NPT ensemble at 1 bar with the Parinello-Rahman algorithm were employed successively to make the temperature and the pressure equilibrated, respectively. Finally, a MD production runs of 100 ns were performed starting from random initial velocities and applying periodic boundary conditions. The non-bonded interactions were treated using Verlet cut-off scheme, while the long-range electrostatic interactions were treated using particle mesh Ewald (PME) method. The short-range electrostatic and van der Waals interactions were calculated with a cut-off of 12 Å. Average structure of the four complexes were generated using the last 10 ns frames and ΔG between the antibodies and RBD was estimated in ROSETTA by InterfaceAnalyzer. Atomic_burial_cutoff,

sasa_calculator_probe_radius and interfaces_cutoff values were set to 0.01, 1.4 and 8.0 respectively.

In vivo protection against SARS-CoV-2 Beta and Omicron variants challenge in mice

The *in vivo* protection efficacies of single antibody or antibody cocktails were assessed by using a newly established mouse model based on a SARS-CoV-2 Beta variant strain [28]. Briefly, groups of 8-month-old female BALB/c mice were infected with 1×10^4 PFU of SARS-CoV-2 Beta variant strain, then infected mice were treated intraperitoneally with a single dose of different antibodies or antibody cocktails (5 mg/kg) at 1 hour after infection. The protection efficacy of XGv347 was also assessed by using 10-week-old K18-hACE2 mice, each challenged with 1×10^2 $TCID_{50}$ of Omicron strain. And two 2 hours post infection, mice were intraperitoneally treated with a single dose of XGv347 at 30 mg/kg or the same volume of PBS as control. The lung tissues of mice from both two groups were collected at 5 dpi for viral RNA loads assay and pathological examination. All mice were randomly allocated in each group.

Viral burden determination

Viral burden in lung from mice were measured as described previously [17]. Briefly, lung tissue homogenates were clarified by centrifugation and viral RNA was extracted using the QIAamp Viral RNA Mini Kit (Qiagen). Viral sgRNA quantification in each tissue sample was performed by quantitative reverse transcription PCR (RT-qPCR) targeting the S gene of SARS-CoV-2. RT-qPCR was performed using One-Step PrimeScript RT-PCR Kit (Takara).

Histology, and RNA in situ hybridization (RNA ISH)

Lung tissues from mice were fixed with perfusion fixative (formaldehyde) for 48 h, and embedded in paraffin according to standard histological assays. For histopathology, lung tissues were stained with hematoxylin and eosin (H&E). Images were captured using Olympus BX51 microscope equipped with a DP72 camera. For RNA ISH assays were performed with an RNAscope 2.5 (Advanced Cell Diagnostics) according to the manufacturer's instruction. Briefly, formalin-fixed paraffin-embedded tissue sections of 5 μm were deparaffinized by incubation for 60 min at 60 ºC. Endogenous peroxidases were quenched with hydrogen peroxide for 10 min at room temperature. Slides were then boiled for 15 min in RNAscope Target Retrieval Reagents and incubated for 30 min in RNAscope Protease Plus before probe

hybridization. The probe targeting 2019-nCoV RNA was designed and synthesized by Advanced Cell Diagnostics (catalog no. 848561). Tissues were counterstained with Gill's hematoxylin and visualized with standard bright-field microscopy. Original magnification was 10×.

Reporting summary

Further information on research design is available in the Nature Research Reporting Summary linked to this paper.

Data availability

The atomic coordinates of XGv347 in complex with S trimer (state 1), XGv347 in complex with S trimer (state 2), XGv347 in complex with S trimer (state 3), XGv347-S have been submitted to the Protein Data Bank with accession numbers: 7WEA, 7WEC and 7WEB, respectively. Furthermore, the atomic coordinates of XGv265, XGv282 and XGv289 have been deposited in the protein data bank under accession code 7WE8, 7WE7 and 7WE9, respectively. Cryo-EM density maps in this study have been deposited at the Electron Microscopy Data Bank with accession codes EMD-32444 (state 1), EMD-32446 (state 2) and EMD-32445 (state 3), EMD-32441 (XGv282), EMD-32442 (XGv265), and EMD-32443 (XGv289). To reveal structural details of Fab binding mechanism, the local optimized method was used to optimized data progress and the related atomic models and EM density maps of optimized reconstructions of Fab interaction interface has been deposited under accession code 7WEE (XGv265), 7WED (XGv347), 7WLC (XGv282), 7WEF (XGv289), EMD-32447 (XGv347), EMD-32448 (XGv265), EMD-32581(XGv282), EMD-32449 (XGv289), respectively.

35 Zhou, Y. *et al.* Enhancement versus neutralization by SARS-CoV-2 antibodies from a convalescent donor associates with distinct epitopes on the RBD. *Cell Rep* **34**, 108699, doi:10.1016/j.celrep.2021.108699 (2021).

36 Wang, N. *et al.* Structure-based development of human antibody cocktails against SARS-CoV-2. *Cell research* **31**, 101-103 (2021).

37 Zivanov, J. *et al.* New tools for automated high-resolution cryo-EM structure determination in RELION-3. *elife* **7**, e42166 (2018).

38 Punjani, A., Rubinstein, J. L., Fleet, D. J. & Brubaker, M. A. cryoSPARC: algorithms for rapid unsupervised cryo-EM structure determination. *Nature methods* **14**, 290-296 (2017).

39 Sun, Y. *et al.* Structure-based development of three-and four-antibody cocktails against SARS-CoV-2 via multiple mechanisms. *Cell research* **31**, 597-600 (2021).

Acknowledgements We thank Dr. Xujing Li, Dr. Xiaojun Huang and Lihong Chen for cryo-EM data collection at the Center for Biological imaging (CBI) in Institute of Biophysics for EM work. We also thank Dr. Yuanyuan Chen, Zhenwei Yang and Bingxue Zhou for technical support on SPR. Work was supported by the Strategic Priority Research Program (XDB29010000, XDB37030000), CAS (YSBR-010), National Key Research and Development Program (2020YFA0707500, 2018YFA0900801), Beijing Municipal Science and Technology Project (Z201100005420017) and Ministry of Science and Technology of China (EKPG21-09 and CPL-1233). Xiangxi Wang was supported by Ten Thousand Talent Program and the NSFS Innovative Research Group (No. 81921005). Kang Wang was supported by the Special Research Assistant Project of the Chinese Academy of Medical Sciences.

Author contributions X.W., K.W., C.F.Q., C.Q. and Y.W. conceived, designed and analyzed the whole experiment; Y.H., M.L., Y.L. and Lin W. performed authentic virus neutralizing assay; Z.J., Q.L., X.P., J.W., S.L. and W.H. performed the pseudovirus neutralizing assays; K.W., Y.J., L.Q., P.G., Z.C., Y.C. and K.F. performed plasmid construction, protein and antibody expression. Q.Z. and P.Y. performed the BLI assay. L.B., H.C. and Y.D. performed animal experiments and analyzed the results. K.W., L.W., B.Z., L.C., P.L., W.F. and N.W. performed cryo-EM sample preparation, data collection, and processing. all authors analyzed data; X.W., K.W., C.F.Q., C.Q. and Y.W. wrote the manuscript with input from all co-authors.

Competing interests Y.H., Lin W. and M.L. are employees of Sinovac Biotech Ltd. Y.J., P.G. and Y.C. are employees of Acrobiosystems Inc. Other authors declare no competing interests.

Additional information

Supplementary information is available for this paper at

Correspondence and requests for materials should be addressed to Cheng-Feng Qin, Youchun Wang, Chuan Qin or Xiangxi Wang.

Peer review information *Nature* thanks the anonymous reviewers for their contribution to the peer review of this work.

Reprints and permissions information is available at www.nature.com/reprints.

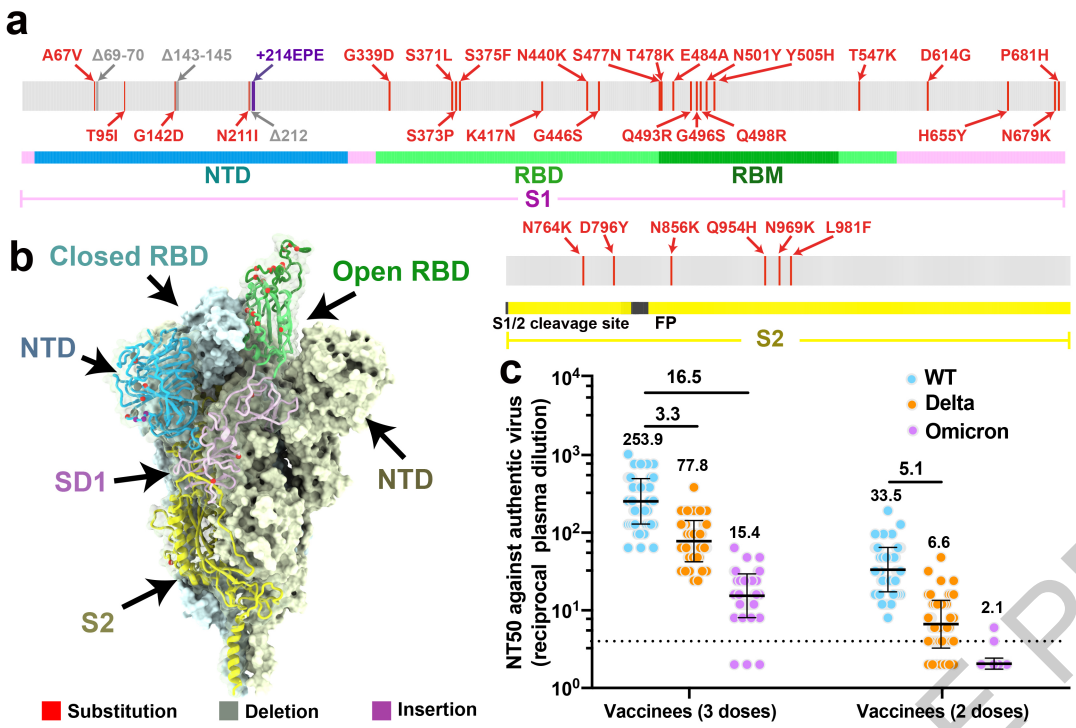

Fig. 1 Evolution and neutralization characteristics of Omicron variant. **a**, A linear representation of Omicron S with mutations marked on. The replacements are marked in red; deletions are in grey and insertions are in purple. **b**, Distribution of mutations of Omicron on the cryo-EM structure of pre-fusion S trimer determined at pH 7.5 (PDB code 7WG6) [34]. The mutations listed in **a** are indicated in the 'up' protomer shown as cartoon with mutated residues highlighted as spheres and colored as in **a**. The RBD, NTD, SD1 and S2 of this subunit are marked with arrow and colored in green, blue, magenta and yellow, respectively; the other two protomers in 'down' state are shown as surface in pale cyan and pale yellow, respectively. **c**, Graph shows the neutralizing antibody response against WT and Omicron SARS-CoV-2 authentic virus for sera from healthy vaccinees who received two doses (n=60 volunteers) or three doses (n=60 volunteers) of Coronavac. Bars and indicated values represent geometric mean of NT_{50} ± SD of technical triplicates. The dotted line represents the detection limit. NT_{50} values less than 4 were plotted as 2. shown above each plot Neutralizing antibody titer fold decline for Delta or Omicron over WT for each group of sera is shown in each of the plots.

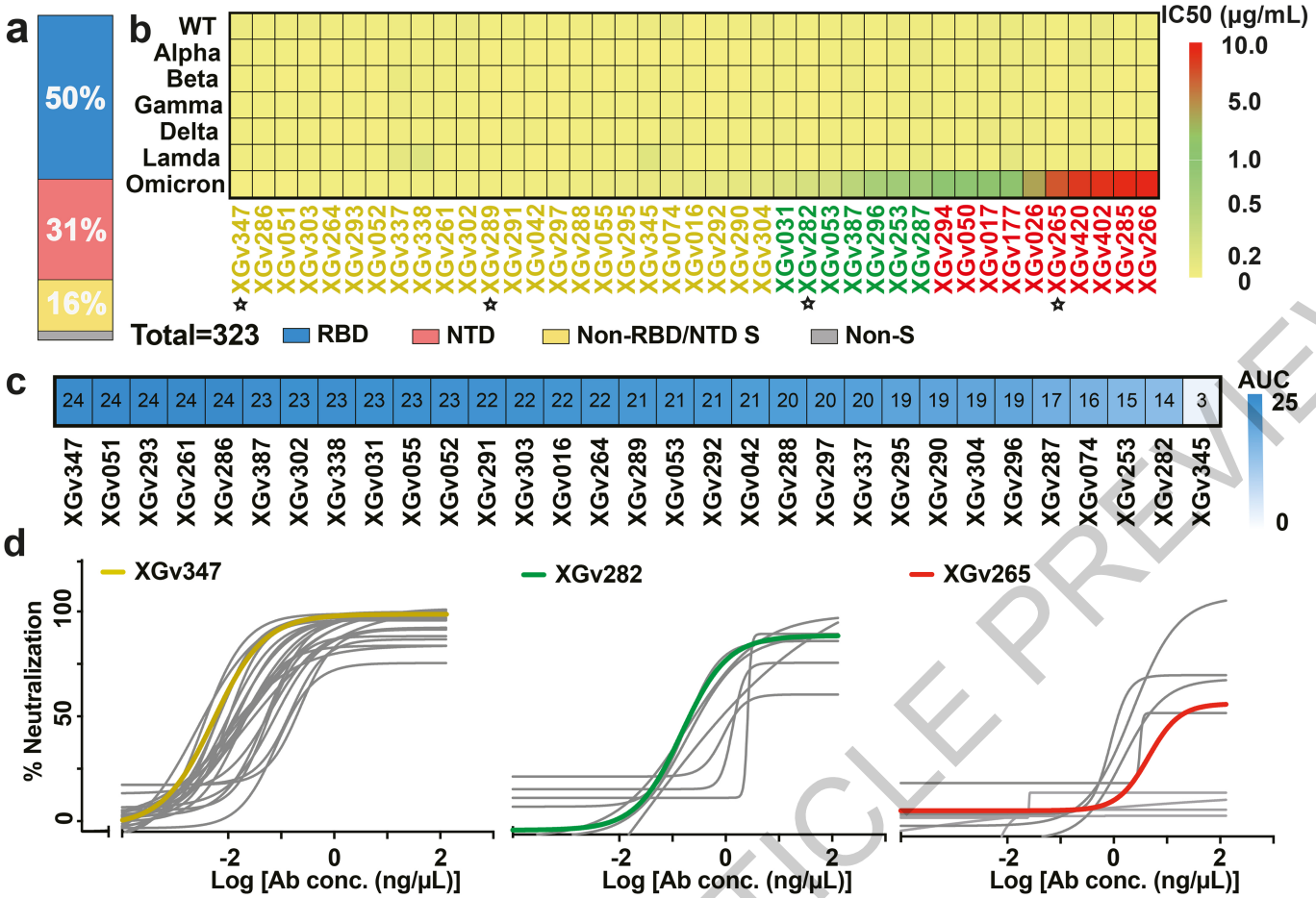

Fig. 2 Characteristics of a subset of broadly neutralizing antibodies from recipients of a booster immunization. a, Vertical slices chart shows the gross binding epitope distribution of mAbs isolated from the individuals who received three doses of inactivated vaccines. Total number of antibodies and the percentage of antibodies that recognize RBD (blue), NTD (red) and S2 domain (yellow) are indicated. **b**, Heatmap representation of 41 selected representative mAbs against pseudotyped viruses with WT or variant SARS-CoV-2 S. The color bar on the right represents the ranges of IC_{50} values for the indicated mAbs against pseudotyped viruses in **c** (yellow: 0.002-0.020 μg/ml; green: 0.020-1.000 μg/ml; red: 1.000-10.000 μg/ml). Antibodies marked with star were selected for structural analysis. **c**, Heatmap with values shown in the form of AUC represents the competition ability between the selected mAbs and hACE2. Color gradient ranging from white (1) to blue (24) is shown on the right represents the competition ability from the weakest to the strongest. **d**, Neutralization curves for the selected 41 antibodies on pseudotyped viruses with the S protein of Omicron variant of concern. Data shown here are three groups of antibodies in correspondence with **b**. yellow - ultrapotent antibodies against all five VOCs, green - highly potent antibodies against other four VOCs, but with median neutralizing activities against Omicron, red - highly potent antibodies against other four VOCs, but with weak neutralizing activities against Omicron. XGv347, XGv282 and XGv265, selected as a representative of each group are highlighted by bold curve in yellow, green, and red, respectively. All experiments were performed in duplicate.

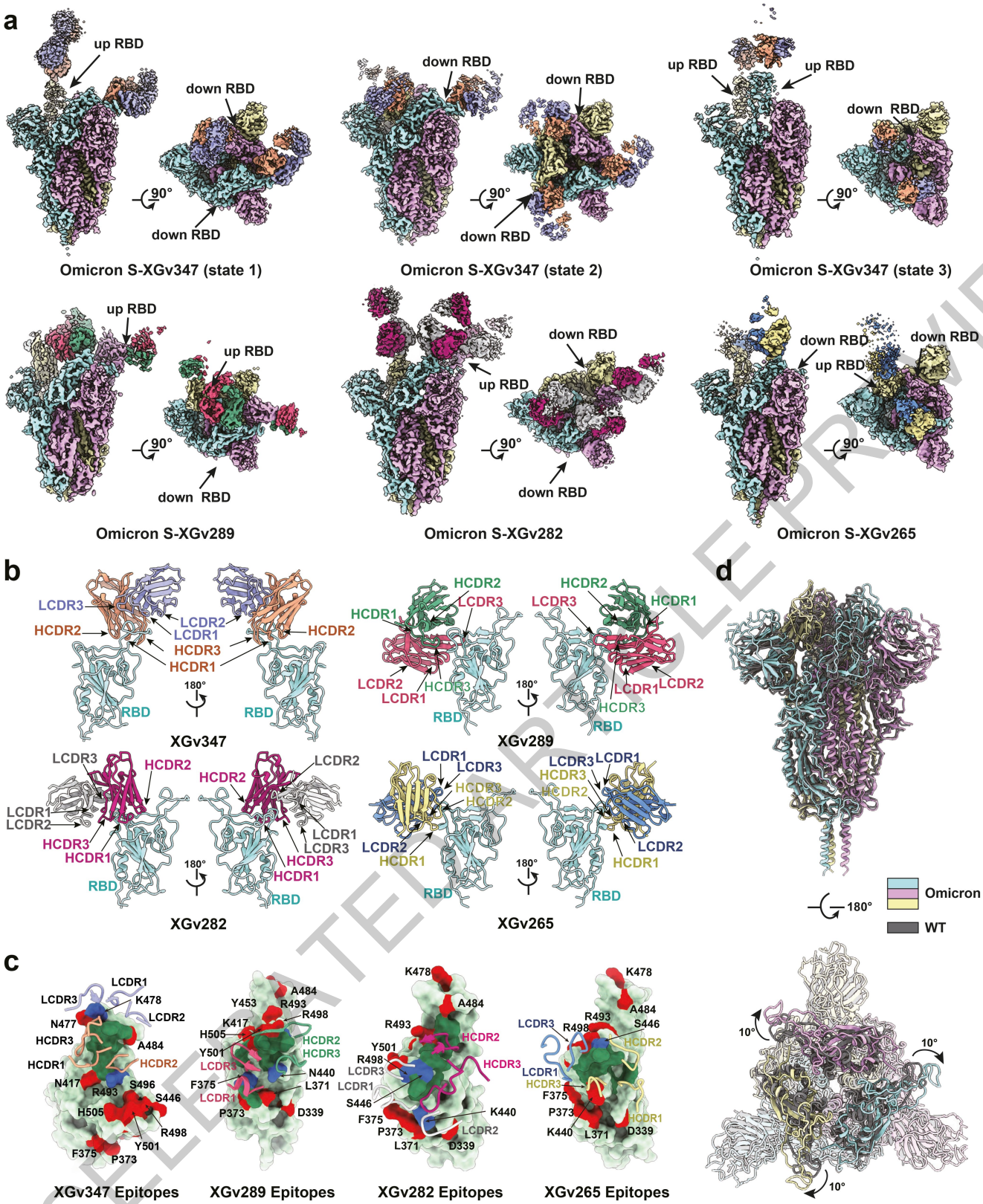

Fig. 3 Structural basis of the broad and potent neutralization of representative antibodies. a. Side view and top view of Cryo-EM maps of SARS-CoV-2 Omicron S trimer in complex with XGv347 (state 1-3), XGv289, XGv282 and XGv265. For XGv347-S-complex, state 1, one up RBD and one down RBD; state 2, three down RBDs; state 3, two up RBDs. **b**. Cartoon representations of the structures of SARS-CoV-2 Omicron-RBD in complex with XGv347 (top-left), XGv289 (top-right), XGv282 (bottom-left) and XGv265 (bottom-right). Two different views for each set are shown to illustrate the binding modes of these four antibodies. RBD is colored in cyan. **c**. Interactions between the four antibodies and SARS-CoV-2 Omicron RBD. The CDRs of the four antibodies that interact with SARS-CoV-2 Omicron RBD are displayed as cartoon over the light green surface of RBD. The mutation sites on RBD of Omicron are colored in red; the epitopes of antibodies are colored in deep green and the overlap of them are colored in blue. Residues of each epitope are marked out in the corresponding regions. d. Superimposition of Omicron onto WT S Trimer. Omicron S trimer is colored in cyan and WT S trimer is colored in yellow.

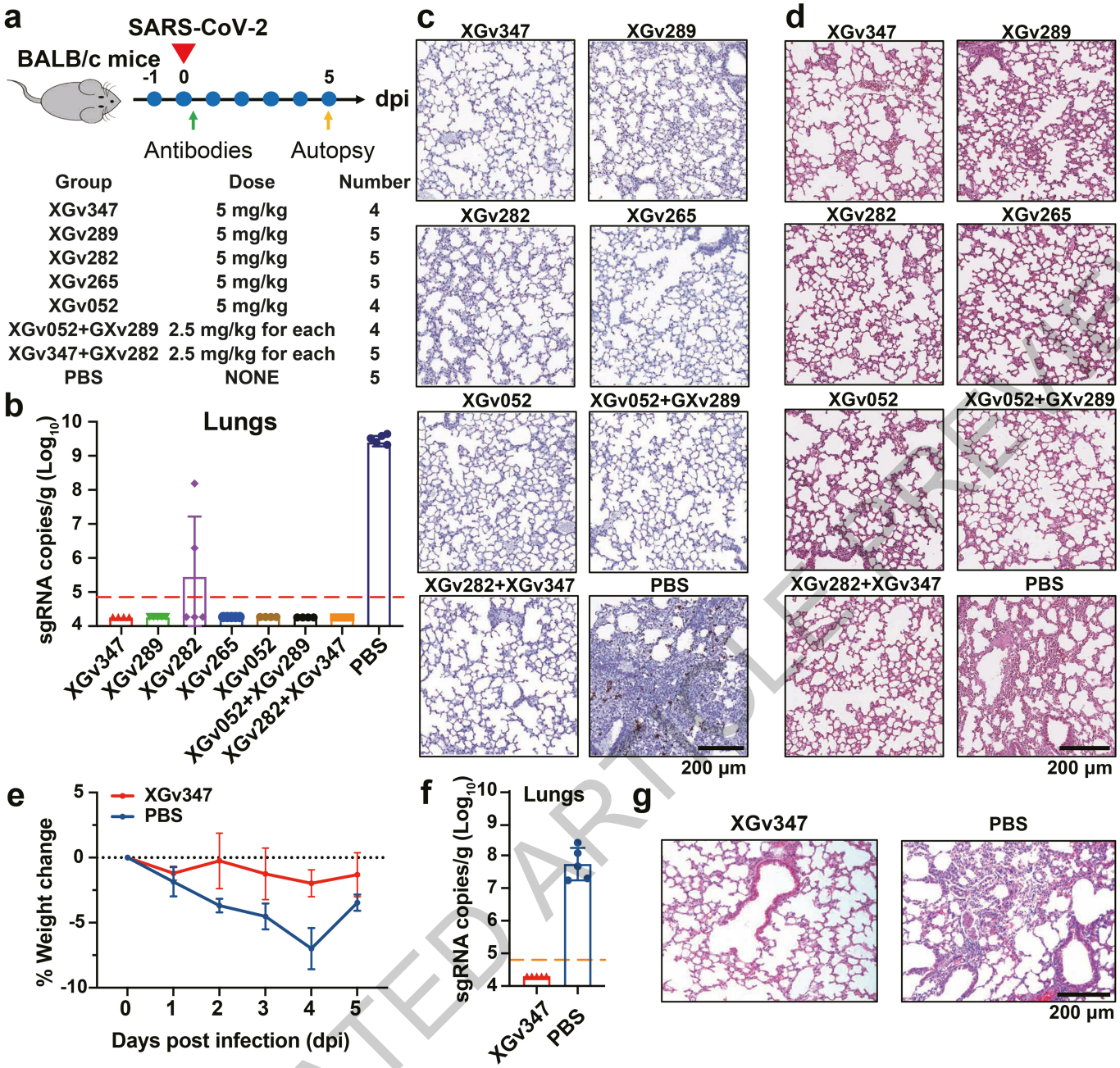

Fig. 4 Protection against SARS-CoV-2 Beta and Omicron variants challenge in mice. a, Experimental design for protection assay against Beta variant challenge. n = 4 mice in XGv347, XGv052, and XGv052 + XGv289 groups; n = 5 mice in other groups. **b to d**, Examination of lung tissues of Beta variant challenged mice collected at 5 dpi for **b**, virus titer, **c**, Immunostaining and **d**, H&E. **b**, Virus RNA loads in the lungs at 5 dpi were measured by RT-qPCR and are expressed as RNA copies per gram. Data are represented as mean ± SD. Dashed line represents limit of detection. **c**, SARS-CoV-2 genome RNA ISH was performed with a SARS-CoV-2 specific probe. Brown-colored staining indicates positive results. Scale bar, 200 μm. **d**, Histopathological analysis of lung samples at 5 dpi. Scale bar: 200 μm. **e to f**, weight change and lung tissues examinations of K18-hACE2 mice challenged with Omicron variant of concern. n = 5 mice in each group. **e**, Weight of each mouse in both groups was monitored and recorded daily post infection. Mean with standard deviation. **f**, Virus RNA loads in the lungs at 5 dpi were also measured as in **b**. Data are represented as mean ± SD**.** Dashed line represents limit of detection. **g**, Histopathological analysis of lung tissues from both two groups. Scale bar, 200 μm. Each micrograph in **c, d and g** is representative of two separate experiments.

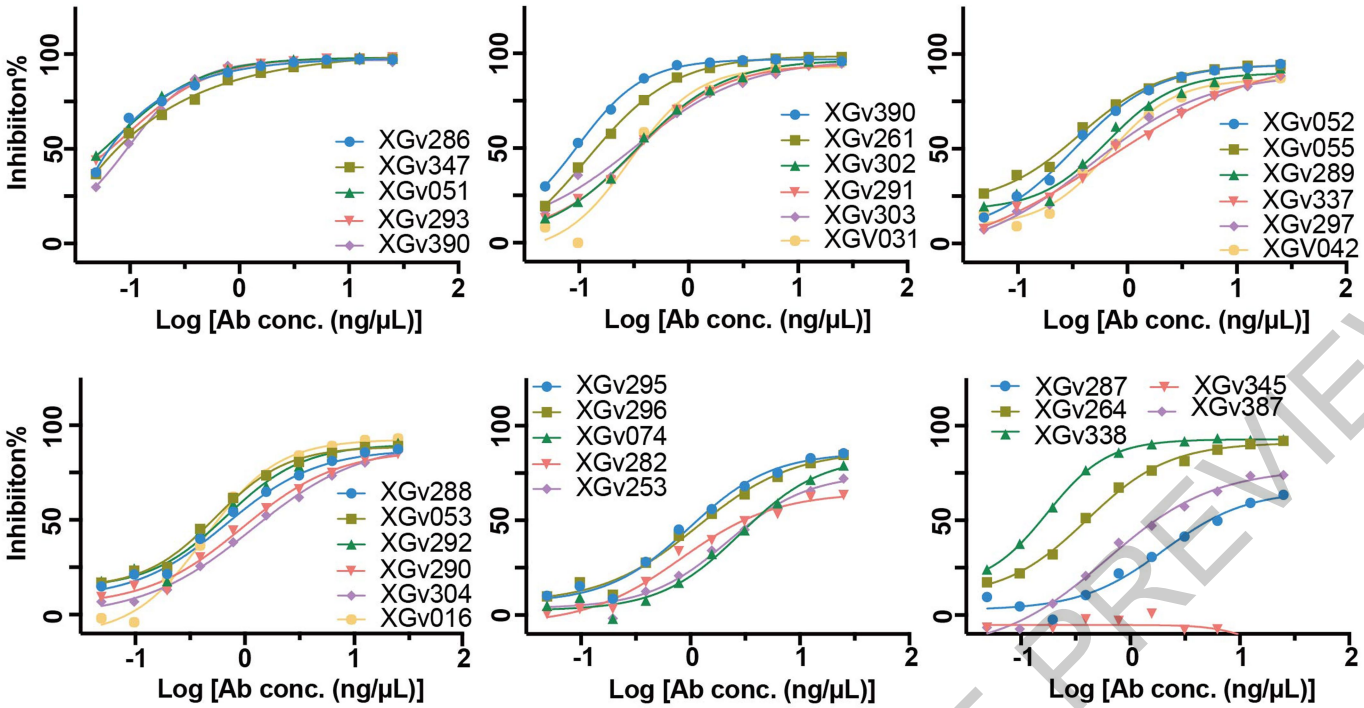

Extended Data Fig. 1 Antibody-hACE2 competition ELISA assay. Data shown are the curves of 31 antibodies used to compete with ACE2. All experiments were performed in duplicate.

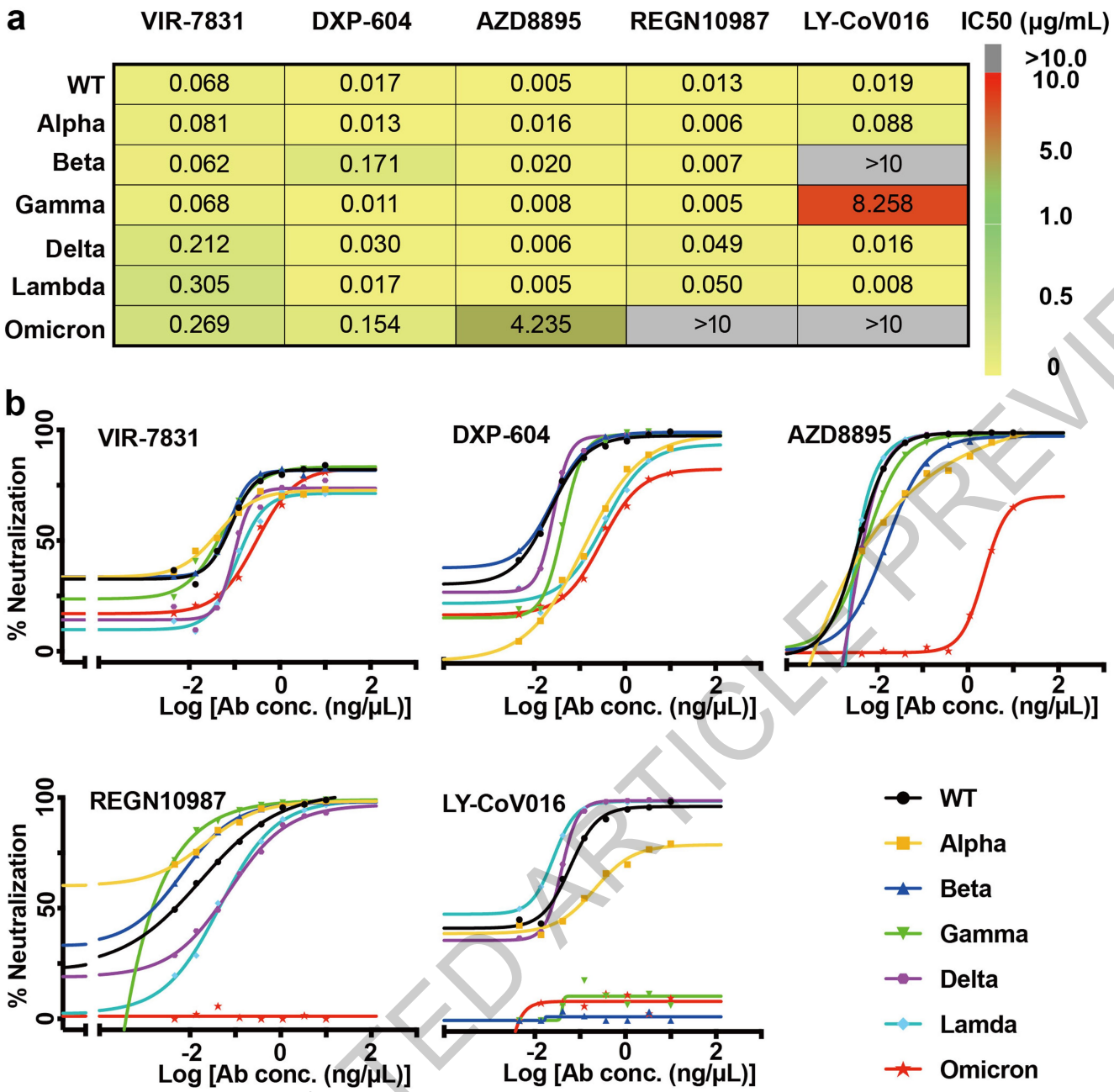

Extended Data Fig. 2 Characteristics of representative antibodies against pseudotyped viruses. a, Heatmap representation of five therapeutic mAbs approved or in clinical trials against pseudotyped viruses with the S proteins of wild-type or variants of concern or interst (Alpha, Beta, Gamma, Delta, Lambda and Omicron). **b,** Neutralization curves for these mAbs in correspondence with **a**. Mean of two experiments is shown.

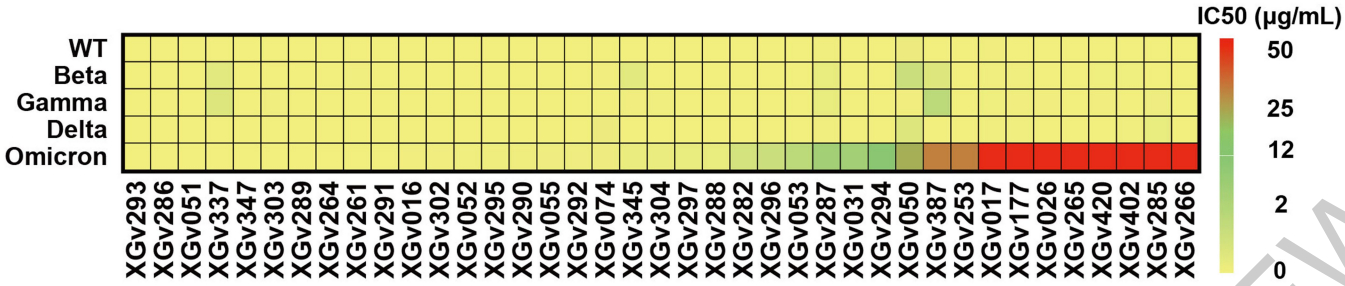

Extended Data Fig. 3 Heatmap representation of representative mAbs against WT and variants of concern. Color bar on the right showed the gradient of IC50 of different antibodies against the authentic WT and variants of concern. All experiments were performed in duplicate.

		Class I				Class II		Class III		Class IV			Class V			Class VI			NC
		XGv013	XGv026	P4A1	XG017	414	H4	XGv031	P17	XGv016	S309	XG014	XGv030	XG025	FC08	XGv004	XG011	A34-2	Fc05
XGv051	1	4	3	3	4	3	9	5	6	94	89	73	71	85	49	325	117	22	101
XGv052	1	3	3	3	3	3	6	4	5	76	55	79	71	86	59	87	66	22	90
XGv053	1	3	5	3	3	3	5	4	7	75	60	76	77	74	57	84	61	22	89
XGv055	1	9	3	3	4	3	9	5	6	89	105	78	83	88	67	321	133	14	95
XGv074	1	5	4	5	5	4	8	7	19	91	61	107	77	89	87	112	80	48	97
XGv253	1	3	3	4	3	3	7	5	5	96	65	80	86	86	81	163	130	145	81
XGv261	1	5	4	3	4	3	9	8	12	91	79	78	71	75	78	272	118	25	94
XGv302	1	3	3	3	4	3	8	7	11	74	73	90	81	90	86	238	144	44	82
XGv303	1	4	4	3	4	3	7	8	13	85	78	92	86	96	89	254	148	47	69
XGv304	1	4	4	4	4	3	7	10	19	89	81	98	83	101	89	237	128	46	99
XGv387	1	6	6	5	4	5	8	15	28	80	63	75	67	60	95	95	74	23	145
XGv177	2	13	18	5	5	5	9	12	27	52	54	67	57	60	87	79	64	24	93
XGv285	2	69	38	78	84	7	10	85	94	43	71	14	72	84	96	94	81	161	107
XGv286	2	41	78	69	73	3	5	80	91	4	88	5	83	77	96	70	90	143	88
XGv287	2	115	81	78	81	15	41	118	104	69	106	32	79	96	96	164	100	133	89
XGv288	2	66	73	69	76	3	7	94	81	5	72	5	69	81	87	77	76	114	91
XGv290	2	65	73	51	76	4	11	81	82	9	60	6	54	77	94	71	69	97	101
XGv291	2	46	72	69	76	3	6	80	83	5	62	4	83	72	92	68	71	127	85
XGv292	2	69	77	62	79	3	5	74	86	7	97	5	81	77	86	75	63	107	86
XGv293	2	42	84	68	80	3	6	88	85	4	79	4	82	82	92	79	73	104	90
XGv294	2	64	78	71	81	3	6	87	88	8	61	5	76	73	87	79	72	96	88
XGv295	2	94	86	74	79	5	11	125	91	9	98	5	91	96	101	280	102	104	106
XGv297	2	57	81	75	76	3	7	101	85	4	76	4	79	72	85	73	79	131	91
XGv338	2	88	85	82	83	3	5	5	4	82	63	47	80	61	5	95	78	100	99
XGv347	2	3	3	3	3	3	7	4	5	88	84	86	96	91	85	256	149	131	97
XGv402	2	9	12	5	7	4	8	23	36	89	63	85	69	73	89	92	74	39	107
XGv420	2	131	88	88	93	3	9	120	51	25	12	5	75	46	64	318	126	57	100
XGv337	3	109	66	77	82	3	9	8	5	79	64	38	67	53	5	277	129	132	94
XGv264	4	63	79	73	84	3	6	93	86	4	5	4	86	72	79	82	84	134	86
XGv265	4	73	77	62	83	3	6	87	86	16	7	5	74	64	80	74	76	108	89
XGv266	4	73	78	87	87	3	5	91	80	12	6	4	85	64	83	86	76	127	86
XGv282	4	81	79	105	77	3	5	83	10	5	43	4	93	76	11	70	89	106	88
XGv289	4	57	78	74	72	3	7	91	77	8	71	5	87	72	82	67	86	143	87
XGv296	4	51	74	64	67	3	6	86	87	5	79	5	80	64	85	67	72	122	87
XGv345	4	88	95	87	92	3	7	97	31	22	7	4	76	12	14	248	132	121	65

Extended Data Fig. 4 Data sheets of ELISA assay of representative mAbs against Omicron RBD. Different Classes of mAbs (Class I-VI) are colored by yellow, green, red, blue, brown and magenta, respectively. Values are filled with black (>75), grey (50-75), silver (25-50) and white (<25). Each data is the mean of three values from three independent experiments.

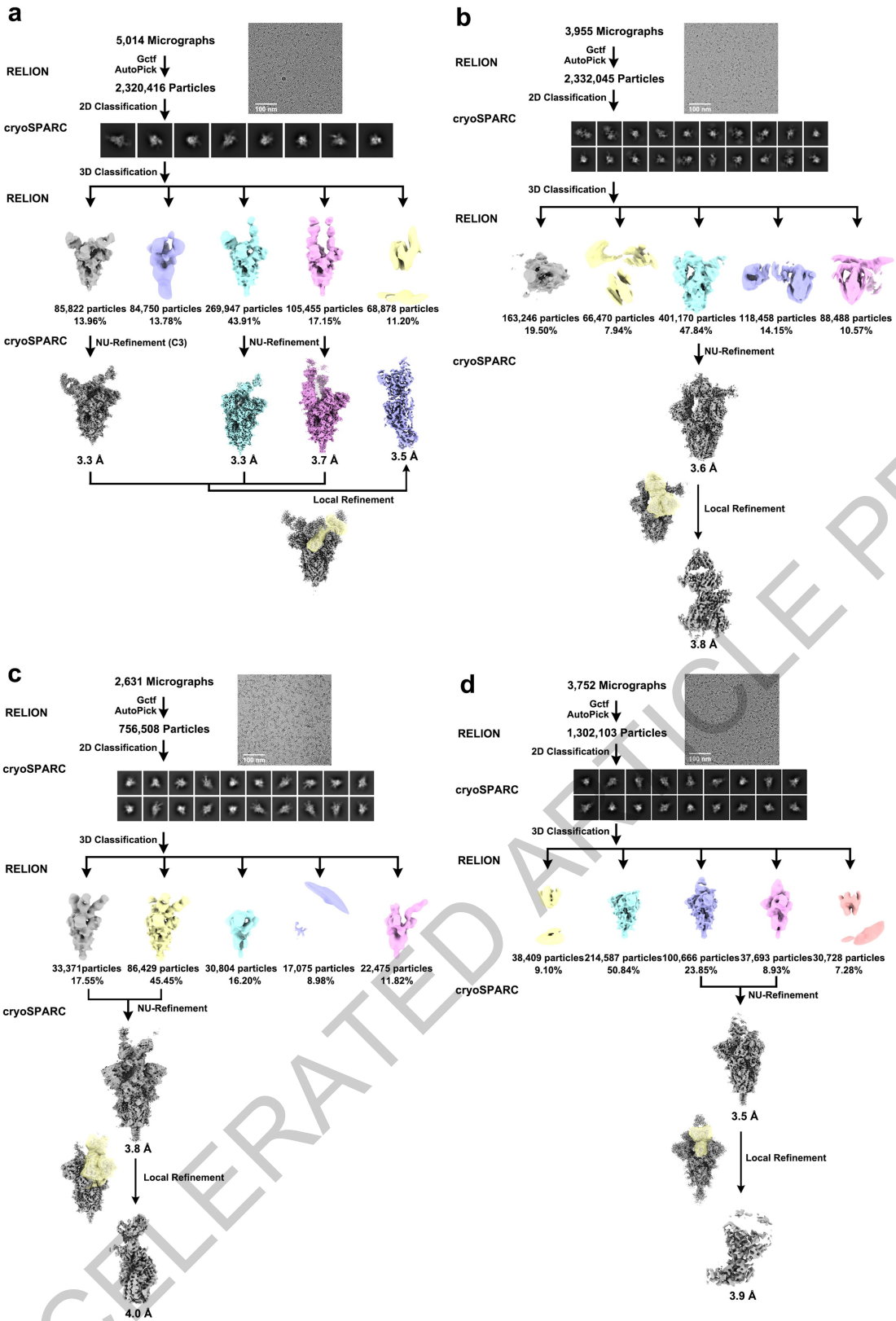

Extended Data Fig. 5 Flowcharts for cryo-EM data processing. Flowcharts for Omicron S protein in complex with **a**, XGv347, **b**, XGv289, **c**, XGv282 and **d**, XGv265 are shown. Scala bar in micrographs, 100 nm.

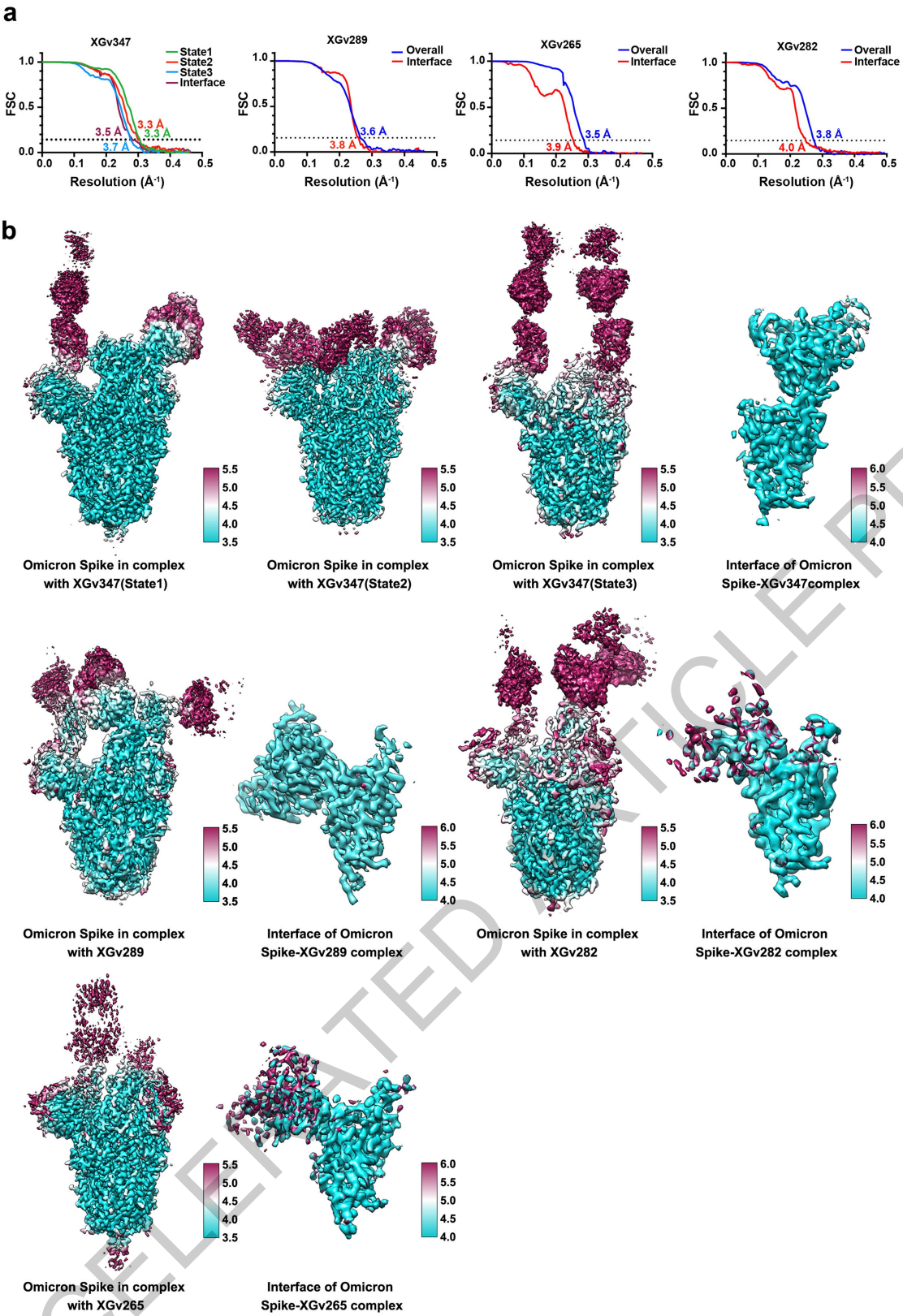

Extended Data Fig. 6 | Resolution estimation of the EM maps. a, The gold-standard FSC curves of overall maps of Omicron S trimer in complex with Fab XGv347, XGv289, XGv282 and XGv265 and local maps of interfaces. **b,** Local resolution assessments of cryo-EM maps using ResMap are shown.

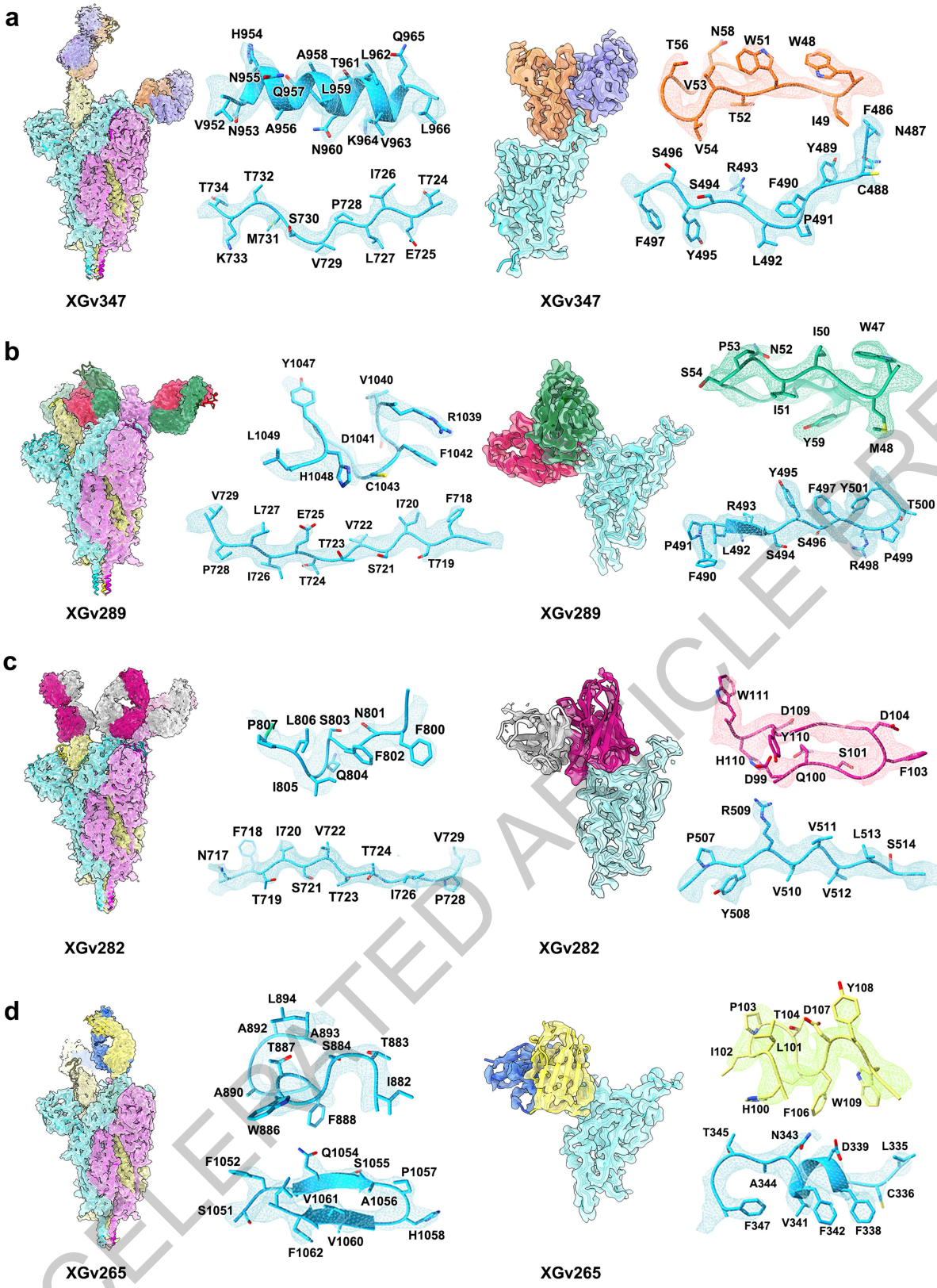

Extended Data Fig. 7 Density maps and atomics models. Cryo-EM density maps of Omicron S trimer in complex with XGv347, XGv289, XGv282 and XGv265 and their interfaces are shown. Color scheme is the same as in Fig. 3**a**. Residues are shown as sticks with oxygen colored in red, nitrogen colored in blue and sulfurs colored in yellow.

Heavy Chain

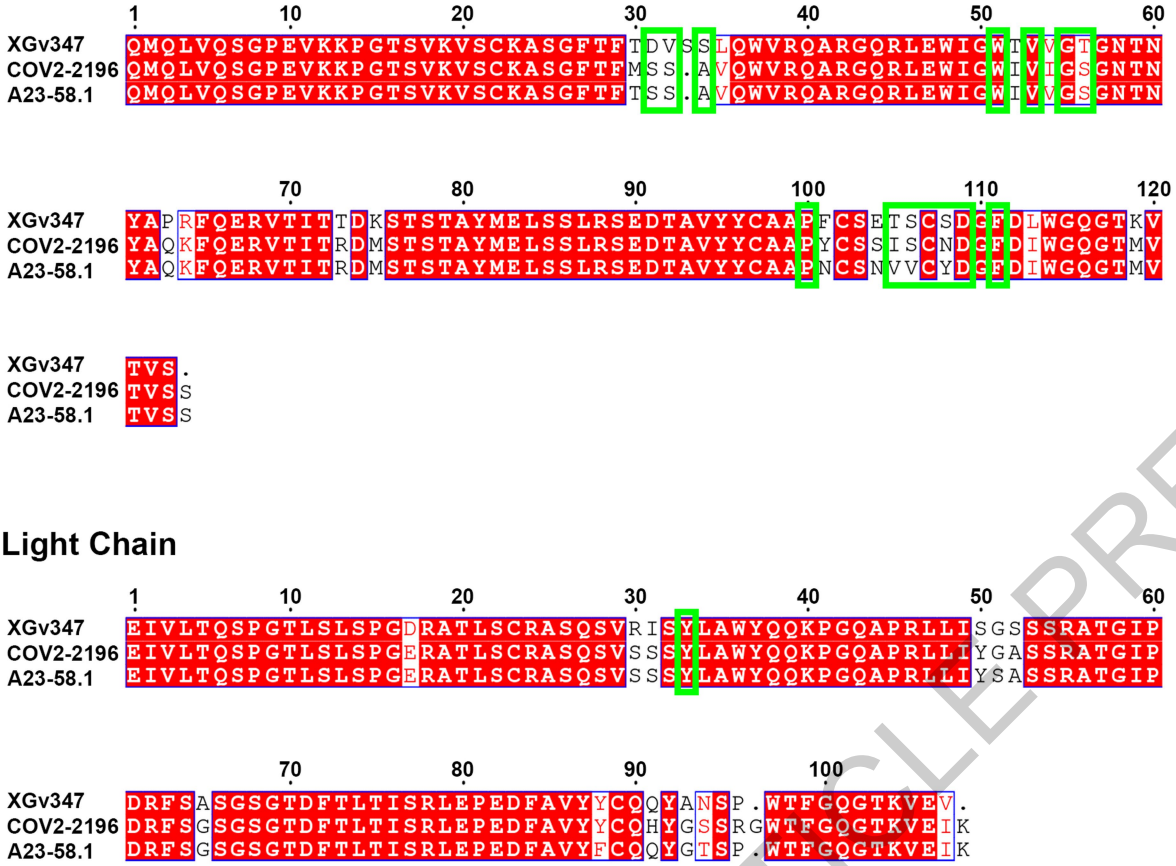

Light Chain

Extended Data Fig. 8 Multiple sequence alignment of XGv347, CoV2-2196 and A23-58.1 Multiple sequence alignments of heavy chains and light chains of XGv347, CoV2-2196 and A23-58.1 were performed, respectively. Paratopes of XGv347 binding to Omicron variant RBD are highlighted by green boxes.

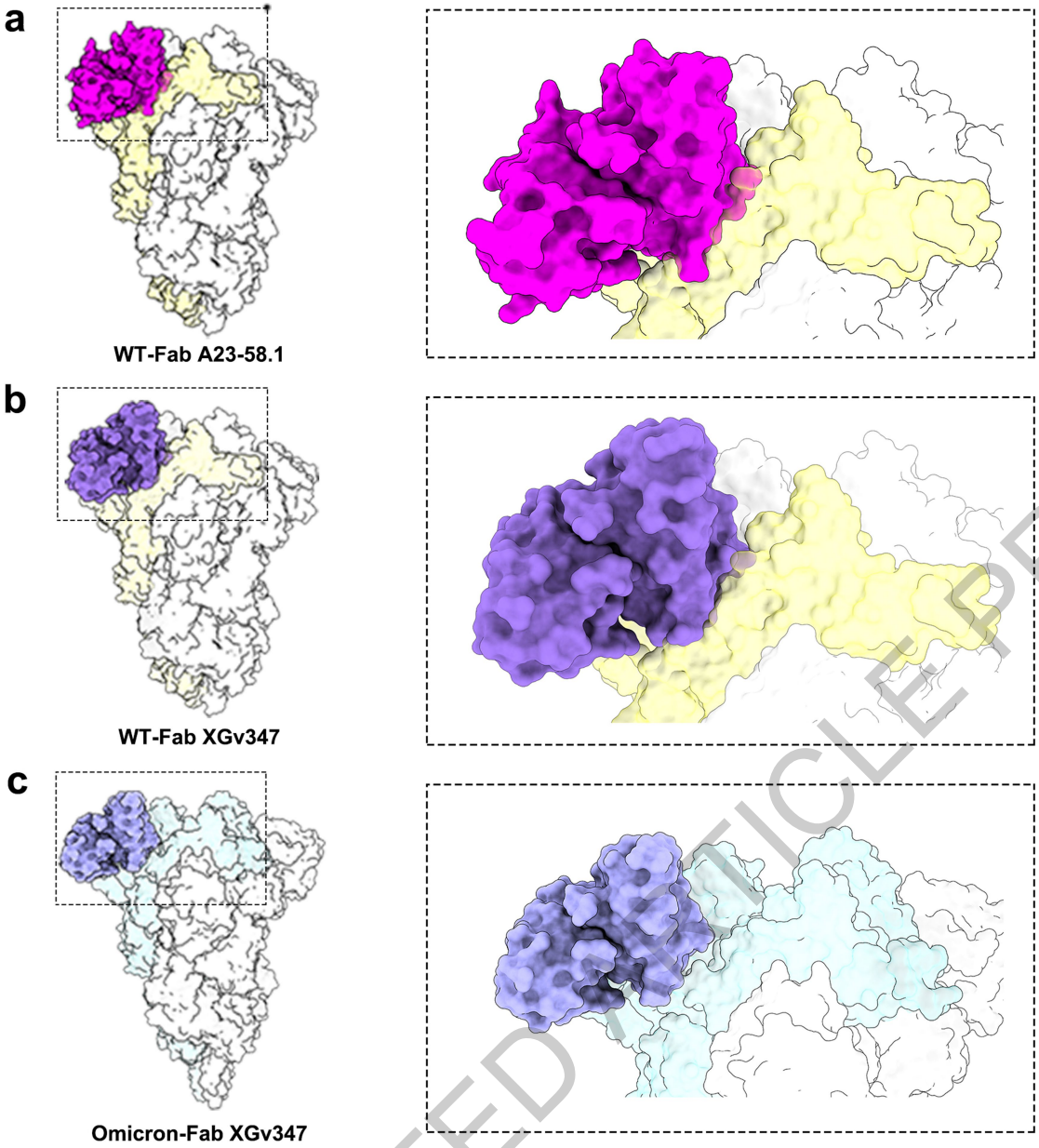

Extended Data Fig. 9 Mechanism of XGv347 binding to 3 closed RBD. a, Superimposition of A23-58.1 onto WT S trimer. **b**, Superimposition of XGv347 onto WT S trimer. **c**, complex of XGv347 and Omicron S trimer. All complexes are in the same orientation with close-ups of Fab-RBD binding modes showing potential clashes.

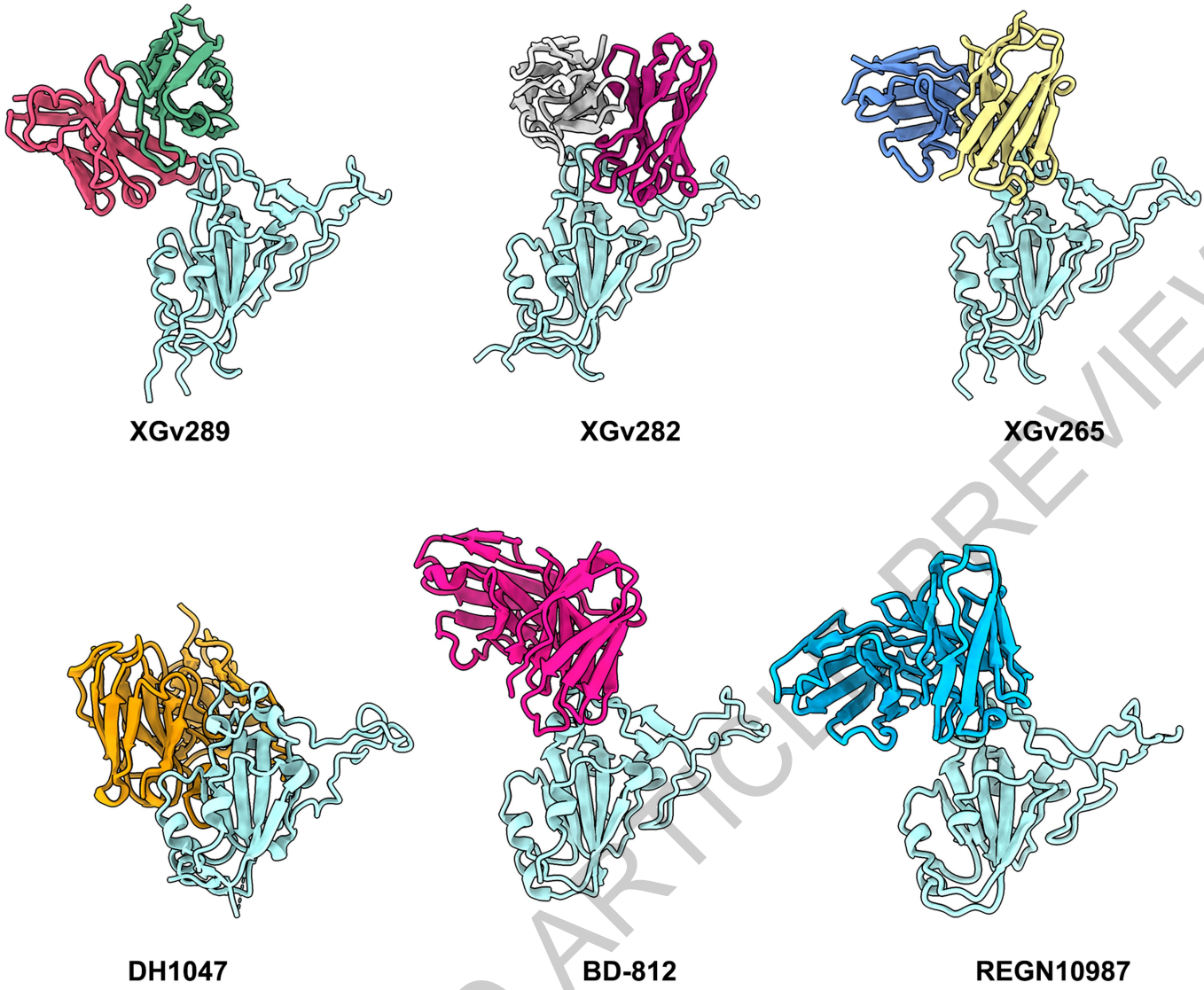

Extended Data Fig. 10 Binding modes of XGv289, 282 and 265. Binding modes of XGv289, XGv282 and XGv265. RBD is colored in light cyan and color scheme of XGv289, XGv282 and XGv265 is the same as in Fig. 3**a**. DH1047, BD-812 and REGN10987 are colored in orange, deep pink and blue, respectively.

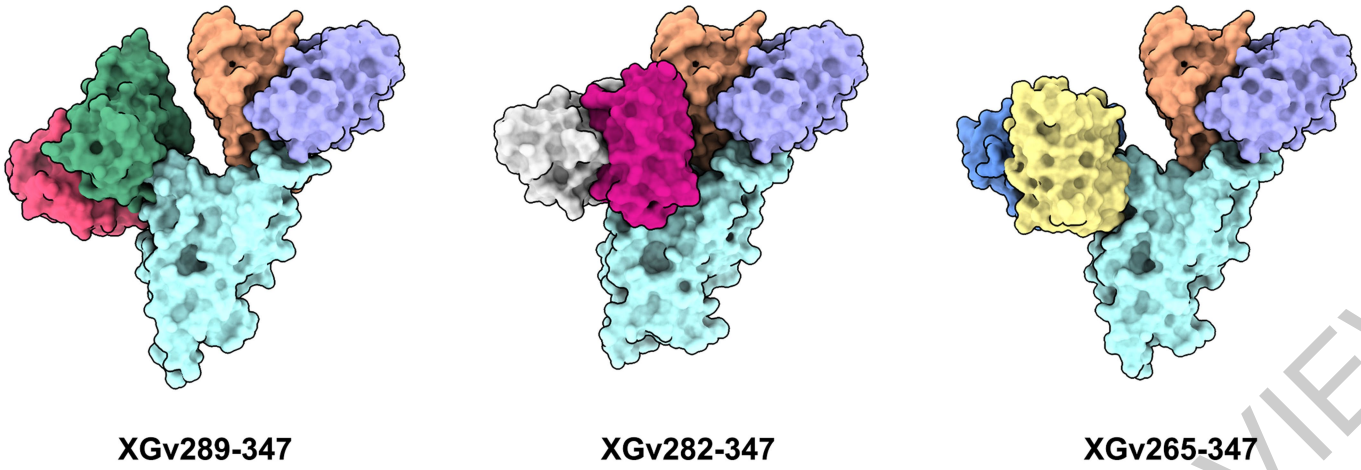

Extended Data Fig. 11 Structural fitting. XGv265, XGv282 and XGv289 are superimposed onto XGv347 and all structure are shown as surface.

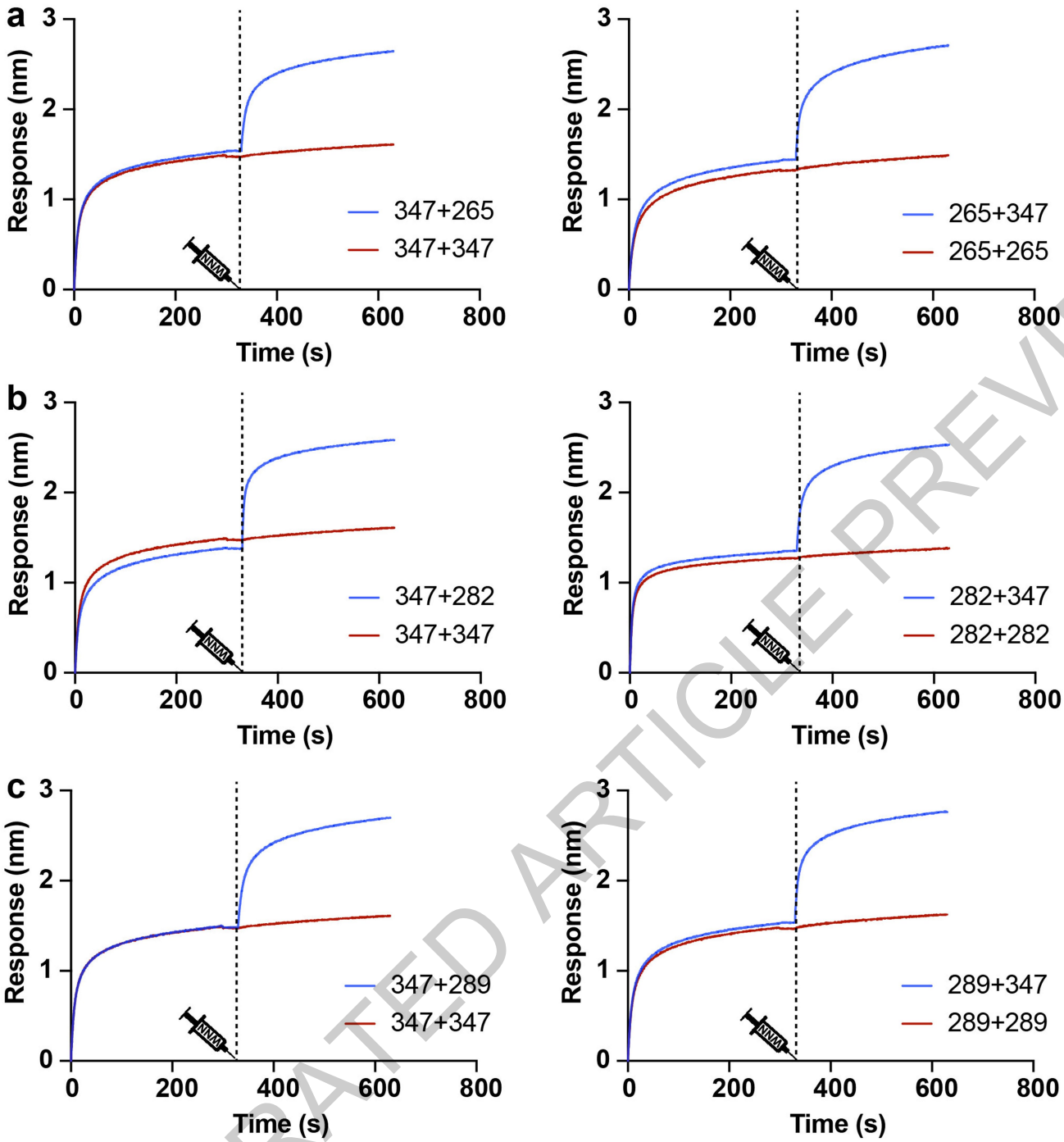

Extended Data Fig. 12 BLI assay for XGv347 competing with XGv289, XGv282 and XGv265. Affinity curves of XGv347 to Omicron S protein competing with **a**, XGv265, **b**, XGv282 and **c**, XGv289. In each panel, (left) XGv347 was first injected, followed by the XGv265, XGv282 and XGv289 in **a**, **b** and **c**, respectively. (right) Also, XGv265 in **a**, XGv282 in **b** and XGv289 in **c**, was injected first and competed with the second injection of XGv347. Each curve is a representative of three independent experiments.

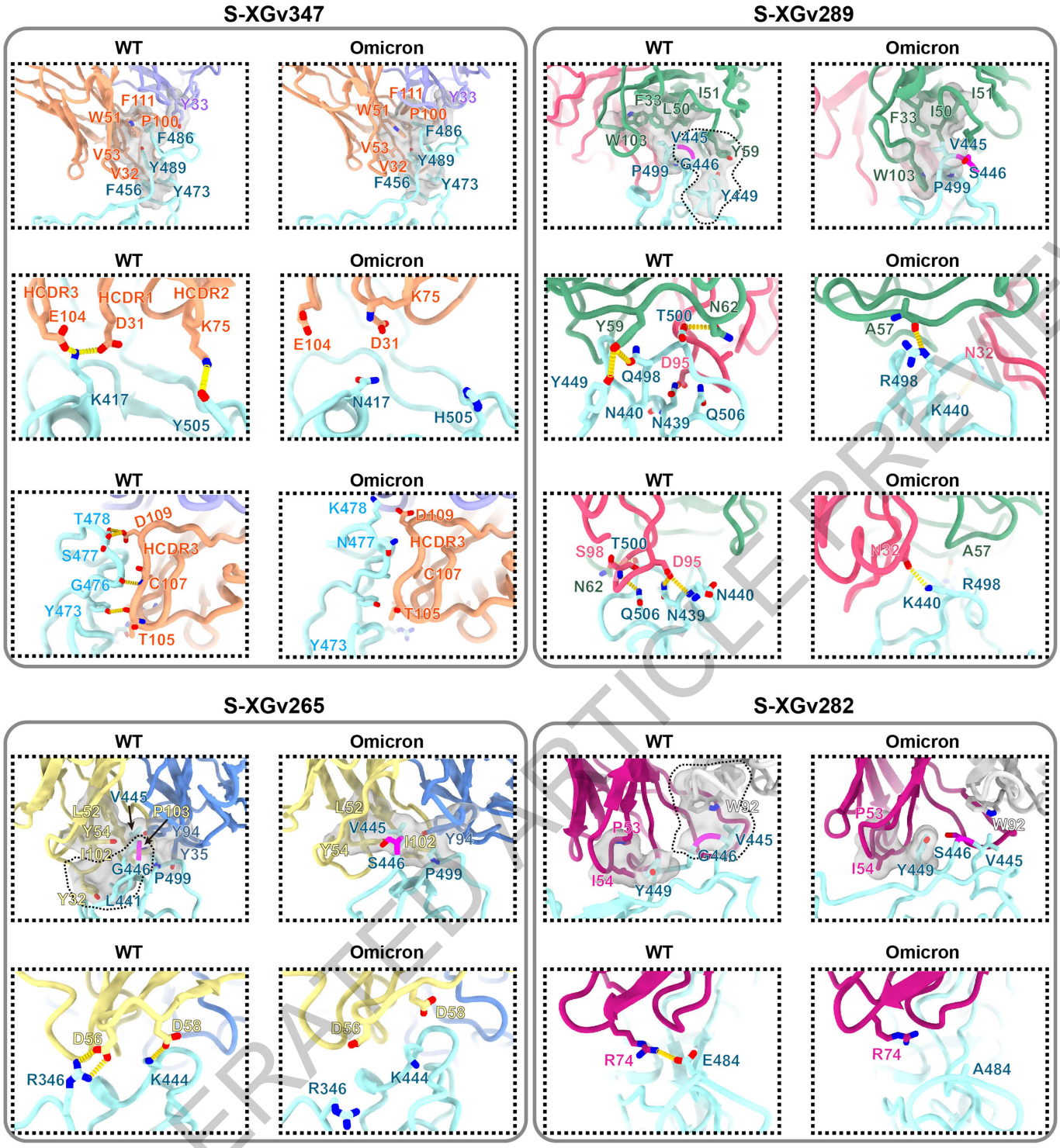

Extended Data Fig. 13 Interactions details between antibodies (XGv347, XGv289, XGv282 and XGv265) and SARS-CoV-2 WT (left) and Omicron RBD (right). All the WT structures are predicted with GROMACS. Hydrophobic patches and hydrogen bonds are denoted by surface and dash lines. Color scheme is the same as in Fig.3**a**. For hydrophobic patches of XGv289, XGv282 and XGv265, G446 and S446 are colored in magenta. The dash lines marked out the hydrophobic patches only found in WT RBD.

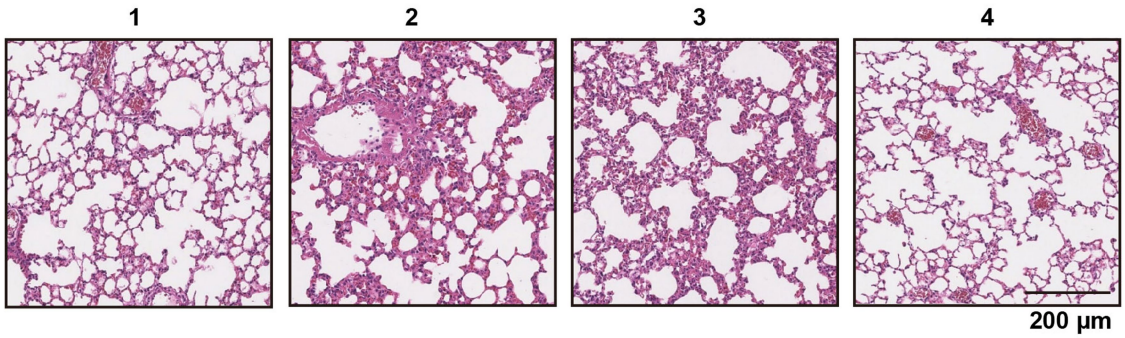

Extended Data Fig. 14 Histopathological analysis of lung samples from XGv282 treatment group at 5 dpi. Shown here are the H&E staining of lung samples from each of the remaining four mice in XGv282 group. Each micrograph is representative of two separate experiments.

	Omicron S trimer in complex with XGv347 (state 1) EMD-32444 PDB 7WEA	Omicron S trimer in complex with XGv347 (state 2) EMD-32446 PDB 7WEC	Omicron S trimer in complex with XGv347 (state 3) EMD-32445 PDB 7WEB	Omicron S trimer in complex with XGv289 EMD-32443 PDB 7WE9	Omicron S trimer in complex with XGv282 EMD-32441 PDB 7WE7	Omicron S trimer in complex with XGv265 EMD-32442 PDB 7WE8	XGv347-RBD-interface EMD-32447 PDB 7WED	XGv289-RBD-interface EMD-32449 PDB 7WEF	XGv282-RBD-interface EMD-32581 PDB 7WLC	XGv265-RBD-interface EMD-32448 PDB 7WEE
Data collection and processing										
Magnification	22,500	22,500	22,500	22,500	22,500	22,500	22,500	22,500	22,500	22,500
Voltage (kV)	300	300	300	300	300	300	300	300	300	300
Electron exposure (e–/Å^2)	60	60	60	60	60	60	60	60	60	60
Defocus range (μm)	-1.5--2.5	-1.5--2.5	-1.5--2.5	-1.5--2.5	-1.5--2.5	-1.5--2.5	-1.5--2.5	-1.5--2.5	-1.5--2.5	-1.5--2.5
Pixel size (Å)	1.07	1.07	1.07	1.07	1.04	1.07	1.07	1.07	1.04	1.07
Symmetry imposed	C1	C3	C1	C1	C1	C1	C1	C1	C1	C1
Initial particle images (no.)	2,320,416	2,320,416	2,320,416	2,332,045	756,508	1,302,103	2,320,416	2,332,045	756,508	1,302,103
Final particles images (no.)	269,947	85,822	105,455	401,170	119,800	138,359	527,413	401,170	119,800	138,359
Map resolution (Å)	3.3	3.3	3.7	3.6	3.8	3.5	3.5	3.8	4.0	3.9
FSC threshold	0.143	0.143	0.143	0.143	0.143	0.143	0.143	0.143	0.143	0.143
Map resolution range (Å)	3.3-60	3.3-60	3.7-60	3.6-60	3.8-60	3.5-60	3.5-60	3.8-60	4.0-60	3.9-60
Refinement										
Initial model used (PDB code)	7CWL	7CWL	7CWL	7CWL	7CWL	7CWL	7CWL	7CWL	7CWL	7CWL
Model resolution (Å)	3.8	3.8	3.8	3.8	3.8	3.8	3.8	3.8	3.8	3.8
FSC threshold	0.143	0.143	0.143	0.143	0.143	0.143	0.143	0.143	0.143	0.143
Model resolution range (Å)	3.8-60	3.8-60	3.8-60	3.8-60	3.8-60	3.8-60	3.8-60	3.8-60	3.8-60	3.8-60
Map sharpening *B* factor (Å^2)	135.7	137.1	134.8	166.0	161.3	165.3	250.0	216.9	200.0	197.2
Model composition										
Non-hydrogen atoms	30,530	32,320	30,488	32,034	31,881	28,730	3,358	3,328	3,307	3,350
Protein residues	3,754	3,984	3,754	3,987	3,981	3,522	431	432	430	429
Ligands	78	81	75	67	61	75	0	0	0	0
B factors (Å^2)										
Protein	109.94	107.91	145.86	120.89	134.24	190.94	54.12	63.36	111.21	59.42
Ligand	127.05	136.95	164.34	142.43	151.94	214.20	-	-	-	-
R.m.s. deviations										
Bond lengths (Å)	0.003	0.003	0.003	0.003	0.003	0.003	0.003	0.003	0.006	0.005
Bond angles (°)	0.590	0.594	0.533	0.563	0.570	0.555	0.700	0.624	1.223	0.720
Validation										
MolProbity score	1.90	1.87	1.87	1.99	1.95	2.00	1.88	1.93	1.81	1.76
Clashscore	9.71	8.88	9.96	10.36	12.49	11.20	6.98	8.46	6.34	8.20
Poor rotamers (%)	0.00	0.00	0.00	0.03	0.06	0.03	0.00	0.00	0.00	0.00
Ramachandran plot										
Favored (%)	94.17	94.07	94.98	92.73	95.08	93.35	91.76	92.49	92.69	95.51
Allowed (%)	5.75	5.90	4.99	7.19	4.92	6.62	8.24	7.51	7.31	4.49
Disallowed (%)	0.08	0.03	0.03	0.08	0.00	0.03	0.00	0.00	0.00	0.00

Extended Data Table. 1 Statistics for cryo-EM data collection, refinement, and validation.

Complex	Omicron RBD	Heavy chain			Light chain		
Omicron S-trimer in complex with XGv265	ARG 346	Y32					
	ASN 439				Y35		
	ASP 442	Y32					
	SER 443	I102					
	LYS 444	Y54	D56	D58	W55		
	VAL 445	Y54	R60	L52		T99	
	SER 446	R60					
	GLY 447	R60					
	PRO 499				Y35	Y94	
	ARG 509	Y32					
Omicron S-trimer in complex with XGv289	PHE 374				N32		
	PHE 375				Y33		
	ASN 439	S101			D95		
	LYS 440	S102	S101		Y33		
	SER 443	S101					
	VAL 445	A57					
	SER 446	A57	S58	G56			
	PRO 499	S101					
	THR 500	N62	A60	Q61		G99	S98
	GLY 502	N62				L97	S98
	VAL 503					D95	S96 L97
Omicron S-trimer in complex with XGv347	LEU 455	D31					
	PHE 456	D31	V32				
	TYR 473	T105					
	ALA 475	S106					
	GLY 476	C107					
	LYS 478	D109					
	GLY 485	W51					
	PHE 486	P100	S108	D109	F111	Y33	
	ASN 487	S108					
	TYR 489	V32	S34	V53			
	ARG 493	G55	T56				
Omicron S-trimer in complex with XGv282	K440	F103					
	S443	F103					
	K444	G102					
	V445	G102	F103	D104		W92	
	S446	G102					
	Y449	S31	R50	I52	I54		
	L452	I54					
	F490	R74					
	R498					W92	

Extended Data Table. 2 List of interacting residues between Fabs and Omicron SARS-CoV-2 S trimer (d < 4 Å).

Complex	KD (nM)	ΔG (kcal/mol)	ΔΔG (kcal/mol)	No. (residue$_{TOTAL}$)	No. (residue$_{RBD}$)	No. (residue$_{Fab}$)	No. (HB or SB)	No. (nonpolar residue$_{RBD}$)	No. (nonpolar residue$_{Fab}$)
WT RBD in complex with XGv265	1.475	-3.99	-0.96	21	10	11	14	4	7
Omicron RBD in complex with XGv265	28.52	-3.03		21	10	11	9	3	7
WT RBD in complex with XGv282	0.8612	-3.79	-1.82	28	15	13	13	7	8
Omicron RBD in complex with XGv282	4.096	-1.97		19	8	11	7	3	8
WT RBD in complex with XGv289	1.287	-5.94	-0.79	21	9	12	16	4	6
Omicron RBD in complex with XGv289	14.17	-5.15		26	11	15	12	3	4
WT RBD in complex with XGv347	0.1518	-5.42	-0.14	23	10	13	15	4	5
Omicron RBD in complex with XGv347	6.812	-5.28		26	11	15	9	4	5

Extended Data Table. 3 Statistics for molecular dynamics.

HB, hydrogen bond; SB, salt bridge.

nature portfolio

Corresponding author(s): Xiangxi Wang

Last updated by author(s): Jan 12, 2022

Reporting Summary

Nature Portfolio wishes to improve the reproducibility of the work that we publish. This form provides structure for consistency and transparency in reporting. For further information on Nature Portfolio policies, see our Editorial Policies and the Editorial Policy Checklist.

Statistics

For all statistical analyses, confirm that the following items are present in the figure legend, table legend, main text, or Methods section.

n/a	Confirmed
☐	☒ The exact sample size (*n*) for each experimental group/condition, given as a discrete number and unit of measurement
☐	☒ A statement on whether measurements were taken from distinct samples or whether the same sample was measured repeatedly
☒	☐ The statistical test(s) used AND whether they are one- or two-sided *Only common tests should be described solely by name; describe more complex techniques in the Methods section.*
☒	☐ A description of all covariates tested
☒	☐ A description of any assumptions or corrections, such as tests of normality and adjustment for multiple comparisons
☐	☒ A full description of the statistical parameters including central tendency (e.g. means) or other basic estimates (e.g. regression coefficient) AND variation (e.g. standard deviation) or associated estimates of uncertainty (e.g. confidence intervals)
☒	☐ For null hypothesis testing, the test statistic (e.g. *F*, *t*, *r*) with confidence intervals, effect sizes, degrees of freedom and *P* value noted *Give P values as exact values whenever suitable.*
☒	☐ For Bayesian analysis, information on the choice of priors and Markov chain Monte Carlo settings
☒	☐ For hierarchical and complex designs, identification of the appropriate level for tests and full reporting of outcomes
☒	☐ Estimates of effect sizes (e.g. Cohen's *d*, Pearson's *r*), indicating how they were calculated

Our web collection on statistics for biologists contains articles on many of the points above.

Software and code

Policy information about availability of computer code

Data collection	Serial EM3.8
Data analysis	GROMACS2021,RELION 3.0, cryoSPARC 3.3.1, Chimera 1,15, Chimerax 1.1, coot0.9.4, Phenix 1.19 and GraphPad Prism 9.2.0 were used for data analysis.

For manuscripts utilizing custom algorithms or software that are central to the research but not yet described in published literature, software must be made available to editors and reviewers. We strongly encourage code deposition in a community repository (e.g. GitHub). See the Nature Portfolio guidelines for submitting code & software for further information.

Data

Policy information about availability of data

All manuscripts must include a data availability statement. This statement should provide the following information, where applicable:

- Accession codes, unique identifiers, or web links for publicly available datasets
- A description of any restrictions on data availability
- For clinical datasets or third party data, please ensure that the statement adheres to our policy

Data availabilityThe atomic coordinates of XGv347 in complex with S trimer (state I), XGv347 in complex with S trimer (state II), XGv347 in complex with S trimer (state III), XGv347-S have been submitted to the Protein Data Bank with accession numbers: 7WEA, 7WEC and 7WEB, respectively. Futhermore, the atomic coordinates of XGv265, XGv282 and XGv289 have been deposited in the protein data bank under accession code 7WE8, 7WE7 and 7WE9, respectively. Cryo-EM density maps in this study have been deposited at the Electron Microscopy Data Bank with accession codes EMD-32444 (state1), EMD-32446 (state2) and EMD-32445 (state3), EMD-32441 (XGv282), EMD-32442 (XGv265), and EMD-32443 (XGv289). To reveal structural details of Fab binding mechanism, the local optimized method are used to optimized data progress and the related atomic models and EM density maps of optimized reconstructions of Fab interaction

interface has been deposited under accession code 7WEE (XGv265), 7WED (XGv347), 7WLC (XGv282), 7WEF (XGv289), EMD-32447 (XGv347), EMD-32448 (XGv265), EMD-32581(XGv282), EMD-32449 (XGv289), respectively.

Field-specific reporting

Please select the one below that is the best fit for your research. If you are not sure, read the appropriate sections before making your selection.

☒ Life sciences ☐ Behavioural & social sciences ☐ Ecological, evolutionary & environmental sciences

For a reference copy of the document with all sections, see nature.com/documents/nr-reporting-summary-flat.pdf

Life sciences study design

All studies must disclose on these points even when the disclosure is negative.

Sample size	No statistical methods were used to predetermine sample size. We obtained 120 human serums, all the vaccine sera were collected from volunteers who received two doses or three doses of the WHO-approved inactivated SARS-CoV-2 vaccine (CorovaVac, Sinovac, China). For the animal study, 37 BALB/c mice and 10 K18-hACE2 mice were used for protection experiments.
Data exclusions	No data excluded.
Replication	All experiments were performed and verified in multiple replicates as indicated in their methods/figure legends.
Randomization	All mice were divided into the given groups (7 for Beta strain challenge and 2 for Omicron strain challenge) randomly.
Blinding	Volunteers received vaccinations open-label. The investigators were not blinded to allocation during experiments and outcome assessment. Data collection and analysis were performed by different people, the sample classification were replaced by simple marks during data analysis

Reporting for specific materials, systems and methods

We require information from authors about some types of materials, experimental systems and methods used in many studies. Here, indicate whether each material, system or method listed is relevant to your study. If you are not sure if a list item applies to your research, read the appropriate section before selecting a response.

Materials & experimental systems

n/a	Involved in the study
☐	☒ Antibodies
☐	☒ Eukaryotic cell lines
☒	☐ Palaeontology and archaeology
☐	☒ Animals and other organisms
☐	☒ Human research participants
☒	☐ Clinical data
☒	☐ Dual use research of concern

Methods

n/a	Involved in the study
☒	☐ ChIP-seq
☒	☐ Flow cytometry
☒	☐ MRI-based neuroimaging

Antibodies

Antibodies used	XGv347,XGv286,XGv051,XGv303,XGv264,XGv293,XGv052,XGv337,XGv338,XGv261,XGv302,XGv289,XGv291,XGv042,XGv297,XGv288, XGv055,XGv295,XGv345,XGv074,XGv016,XGv292,XGv290,XGv304,XGv031,XGv282,XGv053,XGv387,XGv296,XGv253,XGv287,XGv294, XGv050,XGv017,XGv177,XGv026,XGv265,XGv420,XGv402,XGv285,XGv266, VIR-7831, DXP-604, AZD8895, REGN10987, LY-CoV016
Validation	All of the XGv series SARS-CoV-2 spike antigen-specific monoclonal antibodies have been validated for use in ELISA, BLI and neutralizing SARS-CoV-2 pseudovirus/authentic virus first time in this study. S309, VIR-7831, DXP-604, AZD8895, REGN10987, LY-CoV016 have been validated in previous publications cited in this paper. Specifically,VIR-7831 was tested in Pinto, D et al 2020, Nature;DXP-604 was tested in Shuo, D. et al 2020, Cell; AZD8895 was tested in Jinhui,D. et al 2021,Nat Microbiol; REGN10987 was tested in Johanna Hansen et al 2020, Science;LY-CoV016 was tested in Shi, R. et al 2020, Nature.

Eukaryotic cell lines

Policy information about cell lines

Cell line source(s)	HEK293T cells (ATCC, cat. no. CRL-3216), Huh-7 cells (Japanese Collection of Research Bioresources [JCRB], cat. no. 0403),HEK293F cells (Thermo Fisher, cat. no. 11625019)
Authentication	The authentication of cells have been confirmed using STR method

Mycoplasma contamination	These cell lines tested negative for mycoplasma.
Commonly misidentified lines (See ICLAC register)	None

Animals and other organisms

Policy information about studies involving animals; ARRIVE guidelines recommended for reporting animal research

Laboratory animals	Groups of BALB/c and K18-hACE2 mice were used. All mice were group-housed conventionally on a 12-h light/dark cycle for 3 days before any experiments,the environmental conditions were maintained thermostatically between 18°C-23°C with 40%-60% humidity.
Wild animals	No wild animals were used in the study
Field-collected samples	No field collected samples were used in the study.
Ethics oversight	All procedures associated with SARS-CoV-2 live virus were approved by the Animal experiment Committee Laboratory Animal Center, Beijing Institute of Microbiology and Epidemiology with an approval number of IACUC-IME-2021-022 and performed in Biosafety Level 3 (BSL-3) laboratories in strict accordance with the recommendations in the Guide for Care and Use of Laboratory Animals.

Note that full information on the approval of the study protocol must also be provided in the manuscript.

Human research participants

Policy information about studies involving human research participants

Population characteristics	Plasma samples were obtained from volunteers who received two doses or three doses of the WHO-approved inactivated SARS-COV-2 vaccine (CorovaVac, Sinovac, China).Median age of participants was 37 years. 44% of volunteers were males and 56% were females.
Recruitment	All the volunteers were recruited by Sinovac, Inc. None of the volunteers had a history of prior SARS-CoV-2 infection and none reported serious adverse events after vaccination.
Ethics oversight	The procedures about human participants were approved by the Ethics Committee (seal) of Beijing Youan Hospital, Capital Medical University with an approval number of LL-2021-042-K. All participants provided written informed consent.

Note that full information on the approval of the study protocol must also be provided in the manuscript.